Integrated analysis reveals neuro-immune pathway in the central nervous system that supports SGLT2i's protective effects in treatment of cardiac remodeling

First Author: Miao Yuan[1],

Author 1: Hanxue Wu[2],

Author 2: Jiawei Wang[2],

Author 3: Zihan Qiu[2],

Author 4: Kexin Li[1],

Author 5 (co-corresponding author): Jiaxi Xu[1,2,3]

Author 6 (corresponding author): Dengfeng Gao[1],

1 Department of Cardiology, Second Affiliated Hospital of Xi'an Jiaotong University, Xi'an 710004, Shaanxi, China.

2 Department of Physiology and Pathophysiology, Xi'an Jiaotong University, Xi'an 710061, Shaanxi, China.

3 Key Laboratory of Neural and Vascular Biology, Ministry of Education, Hebei Medical University, Shijiazhuang, Hebei, 050017, China.

Dengfeng Gao & Jiaxi Xu are corresponding author of this article. They are all responsible for communicating with the other authors about progress, submissions of revisions and final approval of proofs.

Dengfeng gao: gaomedic@mail.xjtu.edu.cn

Jiaxi Xu: xujiaxi@xjtu.edu.cn

Abstract

Background: Growing evidence are showing beneficial effects of sodium glucose transport protein 2 inhibitors (SGLT2i) in treatment of heart failure, but underlying neurogenic mechanism remains unclear. In this study the effect of empagliflozin (EM) on sympatho-excitation and potential neurogenic mechanism for EM`s therapeutic effects on cardiac remodeling were studied.

Methods: Deoxycorticosterone acetate (DOCA)-salt and high-salt (8%) diet (HSD) mouse models were utilized. Single-cell RNA sequencing was used to explore the mechanism by which SGLT2 inhibitors improve cardiac remodeling in hypertension. Meanwhile, blood samples were collected from hospitalized patients diagnosed with heart failure to verify the results of animal studies.

Results: In DOCA-salt or HSD treated mice, EM was associated with a protective, blood pressure-independent effect on cardiac remodeling. Both DOCA-salt and HSD induced sympatho-excitation, together with neuronal hyper-activity in the pre-autonomic regions of brain, and these were blunted in mice with EM co-treatment. Additionally, single-nucleus RNA sequencing using hypothalami indicated that cellular interplays among the vessels, microglia and inhibitory neurons were involved in the disease- and EM-associated actions. Further analysis of microglia pinpointed a close involvement of peripheral immune activation in disease-associated state transformation of microglia, during DOCA-salt or HSD treatment, including increased lymphocytes count and plasma level of interferon-γ. Differentially

expressed genes in neurons highlighted that EM abolished disease-associated upregulation of protein ubiquitination, which might support imbalance of presympathetic excitatory/inhibitory tones, and vasopressin production. In patients` blood samples, EM was associated with significant elevation of hematocrit value in all groups, and reduction of lymphocytes counts in the patients with high NT-proBNP value (> 2550 pg/mL, no diuretic co-treatment).

Conclusions: Our data provide a neuro-immune pathway by which EM blunts disease-associated cardiac sympathetic tone and hypertrophic remodeling.

Keywords: Hypertension; Sodium glucose transport protein 2 inhibitors; Central nervous system; Cardiac remodeling

1. Background:

Cardiac remodeling refers to adaptive changes of the heart, in the perspective of structure and systolic function, following physiological or pathological stimuli[1]. Recently, sodium-glucose co-transporter 2 inhibitors (SGLT2i) have shown beneficial effect in the treatment of heart failure[2-4]. The mechanism of action of SGLT2i has been extensively studied, including its impact on cardiac metabolism, energy consumption, and direct effects on cardiac structure and function[5, 6].

Although multiple mechanisms of action of SGLT2i have been reported, the possibility of SGLT2i acting through the autonomic nervous system, especially the sympathetic nervous system, has not been fully dissected. The sympathetic nervous system plays a key role in the occurrence and development of cardiac diseases[7]. It affects heart contractility and heart rate by releasing catecholamines such as epinephrine and norepinephrine. Beyond the heart, sympathetic nerves also innervate other organs that contribute to pathological development of cardiac remodeling, such as the kidney and spleen[8-13]. On one hand, elevation of renal sympathetic activity reduces renal blood flow, induces release of renin and aldosterone, thus increases water-sodium retention. On the other, elevation of sympathetic tone in the immune organs, leads to deployment of lymphocytes from the spleen[13], and enhances myeloid cell generation and leukocyte output in the bone marrow[14, 15]. Renin-angiotensin-aldosterone system (RAAS) has been shown to induce pro-inflammatory

transformation of leukocytes and aggregation of T lymphocytes[16], to exacerbate inflammatory responses. Within the brain, the paraventricular nucleus of hypothalamus (PVN), a pre-autonomic center, has high capillary density, thin vessel diameter, and complex vascular topology[11, 17-21], providing a possible interface for immune cells and cytokines to further boost sympathetic outflow. Accordingly, integrated effect of blunted sympatho-excitation to these organs could decrease the cardiac afterload, support the reduction of cardiac energy consumption, and attenuate inflammation, therefore blunting pathological development of cardiac remodeling. Interestingly, SGLT2i increases urinary sodium excretion, reduces renal blood flow, stimulates short-term renin secretion, but long-term impact on renin and aldosterone is not observed[22, 23]. Clinically, SGLT2i is often applied with diuretics or RAAS inhibitors[23]. Investigating how SGLT2i alone affect central regulation of sympathetic tone would provide novel insight regarding its mechanism of action in cardiac remodeling, and a new perspective on its clinical application.

In this study, via integrated analysis of deoxycorticosterone acetate (DOCA)-salt and high-salt (8%) diet (HSD) mouse models, together with blood samples collected from hospitalized patients diagnosed with heart failure, a pathway involving communication between the peripheral immune system and central nervous system (CNS), from leukocytes to neurons locating in the pre-autonomic center, was studied as potential neurogenic mechanisms for SGLT2i's beneficial role in treatment of cardiac remodeling.

2. Results:

2.1 Empagliflozin ameliorates cardiac remodeling

In this study, the therapeutic effect of empagliflozin (EM) was studied in both DOCA-salt model and 8% high-salt diet model (HSD). DOCA-salt model (3-week) was utilized for its character that induces salt-sensitive type of hypertension and does not elevate circulating renin and angiotensin levels[24-27], while HSD (8-week) was used because it increases salt-intake but cannot induce hypertension in C57BL6/J mice[28-30]. Meanwhile, hydralazine was provided to a subgroup of DOCA-salt-treated mice (DOCA+Hyd) to evaluate the impact of blood pressure. Firstly, there was no significant difference in body weight among the five groups of mice received treatment of DOCA-salt, DOCA+Hyd, DOCA+EM, sham, and sham+EM, respectively (Supplementary Figure1 A). Similarly, no significant difference in body weight was observed among the groups with HSD or normal salt diet (NSD) treatment (Supplementary Figure1 B). EM co-treatment did not affect drinking water consumption in DOCA-salt-treated mice but slightly increase water intake in mice with HSD (Supplementary Figure1 C-F). In DOCA-salt treated mice, co-treatment of EM did not alter either systolic or diastolic BP, mice with DOCA+EM treatment still exhibited hypertension. Unlike EM, co-treatment of hydralazine markedly lower BP in DOCA-salt-treated mice. HSD did not induce hypertension, and EM co-treatment did not alter BP either (Supplementary Figure1 G-N).

In both DOCA-salt and HSD models, cardiac remodeling was determined. Firstly, increase in ratios of heart weight to body weight or tibia length were observed in both models, indicating cardiac hypertrophy, and co-treatment of EM significantly attenuate modeling-associated increase of heart weight ratios. Notably, co-treatment of hydralazine reduced heart weight ratios, in comparison with control DOCA-salt-treated mice, but their heart weight ratios still significantly higher than mice with EM co-treatment, which showed similar levels as the sham controls (Figure 1A, B). Meanwhile, HSD also induced increase in ratios of heart weight to body weight or tibia length (Figure 1C, D), while co-treatment of EM significantly lowered these ratios. Additionally, cardiac remodeling was also determined by tissue staining in left ventricle (LV) and echocardiography. Both DOCA-salt and HSD treatments induced hypertrophy of cardiomyocytes, increase of myocardial interstitial and perivascular fibrosis in the LV (Figure 1E, F), heavier LV mass (Figure 1H, J), as well as significant Collagen III deposition (Figure 1K, L). DOCA-salt treatment also significantly impaired cardiac systolic function, showing reduced ejection fraction of LV (Figure 1G). Co-treatment of EM significantly blunted LV hypertrophy, reduced LV fibrosis and Collagen III deposition, and importantly preserved cardiac systolic function in both models. Hydralazine did not exhibit similar protective effect as EM co-treatment in the perspective of abolishing pathological cardiac remodeling (Figure 1G, I). To this end, we showed that EM co-treatment has protective effect in

pathological cardiac remodeling induced by DOCA-salt or HSD treatment, and this is not dependent on potential anti-hypertensive effect of EM.

EM increases urinary sodium excretion, so we examined the plasma sodium level and osmolality in each group of mice, to determine whether EM inhibits cardiac remodeling by reducing blood sodium or osmolality. No marked difference was detected regarding the plasma sodium level and osmolality among the groups/treatments (Supplementary Figure2 A-D), but DOCA-salt treatment significantly reduced the value of hematocrit (HCT). HCT values can be utilized to represent changes in blood volume, and its reduction in DOCA-salt-treated mice suggests increase of blood volume (Supplementary Figure2 E). Co-treatment of EM, rather than hydralazine, recovered the HCT value to the baseline levels. we tested the HCT of different groups. Unlike DOCA-salt model, HSD did not induce alteration in the value of HCT (Supplementary Figure2 F).

2.2 Empagliflozin blunts sympatho-excitation

To evaluate sympatho-excitation, the levels of urinary norepinephrine (NE), which had been normalized by creatinine (Cr) concentrations, were firstly determined. Additionally, we analyzed urinary, which was used to standardize the urinary NE. As reported previously, DOCA-salt treatment dramatically elevated urinary NE level (Figure2 A), which was not affected by co-treatment of hydralazine, but significantly lowered by co-treatment of EM. Similar to DOCA-salt treatment, HSD boosted urinary NE level as well, and co-treatment of EM reduced its level (Figure2 B). In

addition to global index of sympatho-excitation, expression of tyrosine hydroxylase (TH), a rate-limiting enzyme for NE biosynthesis, was determined to assess sympathetic tone in the LV. DOCA-salt treatment significantly increase TH expression in the LV (Figure2 C-D), which was significantly blunted by co-treatment of EM. Similar as DOCA-salt treatment, HSD increased LV TH expression as well, and this was attenuated by co-treatment of EM (Figure2 E-F).

In the pre-autonomic centers, the PVN and rostral ventrolateral medulla (RVLM), immunofluorescence of c-Fos, the immediate early gene of neuronal activation, was performed to determine modeling-associated neuronal hyper-activity. Co-treatment of EM significantly blunted DOCA-salt- or HSD-induced increase in the number of c-Fos-positive cells (Figure 3), indicating blunted neuronal activation. To this end, we demonstrated that co-treatment of EM reduces neuronal activity in the pre-autonomic centers and blunts modeling-induced sympatho-excitation.

2.3 DOCA-salt and EM co-treatment are associated with vascular immune response in the PVN

To further dissect the potential mechanism by which EM reduces sympathetic activation, PVN tissues from 5 mice/group, in DOCA, DOCA+EM and sham group, were collected for the process of single nucleus RNA sequencing (snRNA-seq) (Figure4 A). A total of 37, 828 cells were obtained in the three groups (Figure4 B). We analyzed labels of the areas adjacent to the PVN, including the anterior hypothalamic area (Pmch+), dorsomedial hypothalamic nucleus (Cck+), medial

preoptic area (Nts+), medial preoptic nucleus (Tac2+), suprachiasmatic nucleus (Lhx1+), and ventromedial hypothalamus (Nr5a1+). The majority of the neurons expressed markers for PVN-locating neurons (Sim+), confirming that we captured the PVN area, and the presence of cells in the lateral, caudal, and anterior of PVN confirmed that our architecture of the extended PVN captured the entire area (Supplementary Figure 3).

Then, we merged cells from the 3 groups and extracted the top 3, 000 highly variable genes for principal component analysis (PCA). The primary components of PCA guided the unsupervised clustering process, resulting in 35 different cell clusters. Linear dimensionality reduction was followed by graph-based unsupervised clustering to achieve this outcome. Uniform manifold approximation and projection (UMAP) was utilized for visualization purposes. We renamed the cell clusters with reference to cellMarker 2.0 and classic marker genes for different cell types. Nine different types of cells were identified from the 35 cell cluster: mature oligodendrocyte (5,854), Excitatory neuron (11,225), Inhibitory neuron (11,390), Mix neuron (4,620), Astrocyte (1,749), Microglial cell (1,444), Immature oligodendrocyte (1,264), Endothelial cell & Pericyte (176), Ependymal cell (106) (Figure4 B, C).

To unveil interactions between these cells alter the excitability of neurons, cell-chat analysis was firstly performed (Figure4 D). We found that DOCA-salt treatment induced direct signaling regulation of microglia by the vascular cells (endothelial cell & pericyte), and this was not observed in the sham control group (upper panel).

Regulation of inhibitory neurons by microglia was detected in both sham- and only DOCA-salt-treated groups, but it was abolished by co-treatment of EM in DOCA-salt-treated group (lower panel). This cell-chat analysis highlighted an important involvement of vascular cells, which were further analyzed for DOCA-salt- or EM-associated differentially expressed genes (DEGs) and the functional enrichment of these DEGs (Figure4 E). Gene ontology (GO) enrichment analysis was performed using DOCA-salt- and EM-associated DEGs, respectively. Both sets of DEGs were found to be significantly related to cytokine signaling and adhesion of immune cells, indicating DOCA-salt might induce immune response to the PVN vessels, therefore increasing recruitment of circulating leukocytes, and this immune response could be abolished by co-treatment of EM (Figure4 F). The PVN has high capillary density, thin vessel diameter, and complex vascular topology[11, 17-21], providing a possible interface for immune cells and cytokines to affect PVN cells. It has been shown that cytokines from leukocytes, such as interferon, has direct impact on microglia[31], the resident immune cell within the brain. The populations of microglia were then extracted and analyzed to confirm the possible impact from peripheral immune cells.

2.4 EM co-treatment abolished reactive transformation of microglia in the PVN

We re-populated and divided the microglia from all groups into four sub-clusters. Following analyzing the top genes of each sub-clusters, they were named according to their major biological process, or reactive state. The 4 sub-clusters were homologous homeostasis microglia (HOM), disease-associated microglia (DAM), interferon

activated microglia (IFN), and microglia associated with myelination (ORM) (Figure5 A, B, C). Next, DOCA-salt- or EM-associated DEGs were analyzed for the HOM, DAM, and IFN clusters (Figure5 D, F, H).

Firstly, the HOM-DEGs that associates with DOCA-salt were mainly enriched in microglial activation, such as G protein-coupled purinergic receptor activity and calcium signaling, indicating upregulated microglial ATP/P_2Y_{12} receptor/Ca^{2+} signaling in the PVN of DOCA-salt treated mice. Interestingly, the HOM-DEGs that associates with EM co-treatment were mostly enriched in the pathway of cell adhesion binding (Figure5 E), suggesting that EM co-treatment might not affect microglia via reducing ATP in the PVN, but directly blunt microglia's interaction with neurons. Secondly, the DAM-DEGs that associates with DOCA-salt were mainly enriched in the pathways of epithelial invasion and phagocytosis, indicating further induced reactive microglia by DOCA-salt, while the DAM-DEGs that associates with EM co-treatment were functionally enriched in platelet activation and oxidative phosphorylation (Figure5 G), indicating altered energy metabolism for microglia. DOCA-salt-induced increase of reactive microglia and EM-related decrease of reactive microglia were validated by reduced co-expression of Iba1 and CD68 in the PVN (Figure6 A, B). Thirdly, the IFN-DEGs that associates with DOCA-salt were mostly enriched in the pathway of efferocytosis, which is significantly influenced by cytokines. The IFN-DEGs that associates with EM co-treatment is highly enriched in

phagocytosis and related pathways (Figure5 I), further confirming that microglia were less reactive in the PVN of mice treated with EM.

Interferon-γ (IFN-γ) is a pro-inflammatory cytokine produced by NK cells, NK T cells, and T cells, and it has been shown to induce disease-associated state transformation of microglia[9, 12, 17, 32-40]. Accordingly, we identified several IFN-DEGs that showed opposite pattern in DOCA-salt and EM co-treated group (Figure5 J), suggesting those IFN-DEGs could be directly related to the protective effect of EM. Notably, *Txndc9*, *Ppia* are related to protection against neuroinflammation damage, while *Adam17* is known for its role in signaling transduction of neuroinflammation and efferocytosis.

Reactive state of microglia was validated by co-staining of Iba1 and CD68. Increased number of reactive microglia was also found in HSD models, and co-treatment of EM significantly blunted HSD-induced increase of microglial reactive transformation (Figure6 C). Additionally, activation of peripheral immune system was determined by lymphocyte counts and plasma level of IFN-γ. DOCA-salt or HSD treatment significantly increased the cell counts of lymphocytes, while co-treatment of EM blunted modeling-induced augment of circulating lymphocytes (Figure6 D, E). Similarly, DOCA-salt or HSD treatment markedly elevated the concentration of IFN-γ in peripheral blood, while this was normalized by co-treatment of EM (Figure6 F, G). In addition to lymphocytes, co-treatment of EM also had impact on neutrophil count caused by high sodium intake (Supplementary Figure3 G, H).

2.5 EM co-treatment was associated with overall blunted neuronal activity in the PVN

Next, snRNA-seq data of neuronal cells were analyzed. For excitatory neurons, DOCA-salt increased the function of PVN neuro-endocrine neurons, meanwhile, it upregulated the ubiquitination pathway of protein degradation (Figure7 A). Co-treatment of EM showed effect on both mechanisms. As to inhibitory neurons, the major effect of DOCA-salt treatment was upregulation of the ubiquitination pathway, while EM co-treatment exhibited significant impact on DOCA-salt-induced protein ubiquitination (Figure7 B), suggesting that EM could help to “calm down” the PVN neuro-endocrine by blunting the pathway of protein ubiquitination. It has been demonstrated that ACE2 ubiquitination impairs its enzymatic activity, thus compromises its ability to support GABAergic inhibitory tone in the PVN[41, 42]. Accordingly, enzymatic activity of ACE2 was measured using hypothalami. As previously reported, DOCA-salt treatment markedly reduced ACE2 activity. On the other hand, EM co-treatment abolished DOCA-salt’s effect on ACE2 enzymatic activity (Figure7 C). Meanwhile, ACE2 activity was also impaired by HSD, and this was prevented by co-treatment of EM (Figure7 D). Furthermore, expression level of NEDD4L, which is responsible for ACE2 ubiquitination during hypertension, was measured. In addition to DOCA-salt hypertension (Figure7 E, F), HSD induced NEDD4L expression as well, and EM co-treatment significantly blunted DOCA-salt or HSD induced upregulation of NEDD4L expression (Figure7 G, H).

ACE2 has showed robust expression in various types of PVN neurons, except for glutamatergic neurons[43, 44]. Then we analyzed PVN neuronal markers to identify which type of neurons response to EM co-treatment. Of note, expression levels of *Oxt*, *Avp*, *Tac1*, *Trh*, and *Sst* were upregulated by DOCA-salt treatment while downregulated by EM co-treatment (Figure7 I), indicating that neuro-endocrine and neurosecretory neurons were involved in the protective effect of EM during DOCA-salt hypertension. To confirm this, plasma co-peptin level was measure, and it showed that DOCA-salt or HSD-related elevation of plasma co-peptin level, was markedly blunted by co-treatment of EM (Figure7 J, K). To this end, we showed that EM co-treatment abolished disease-associated reduction of ACE2 enzymatic activity via affecting ubiquitin-signaling, and this could be result, also a mediator, for less excitation of neuro-endocrine/neurosecretory neurons.

2.6 EM conditionally reduced blood lymphocyte count in patients with heart failure

In mice, we showed that EM conducted protection against cardiac remodeling in DOCA-salt or HSD models possibly via reducing peripheral cytokine-mediated activation of microglia, and reducing excitation of neuro-endocrine/neurosecretory neurons. Next, we designed a cross-sectional observational clinical study, to further validate the above findings in human. We recruited 1864 patients with heart failure were admitted to our hospital and agreed to join this study from January 2018 to January 2023, excluding 675 patients with incomplete hospitalization information or failure to meet enrollment requirements. Our final study population was 1189 patients

with heart failure, divided into a non-treated group (n = 715) and a treated group (n = 474). After propensity score matching (PSM), the study population was divided into a matched non-treated group (n = 437) and a matched treated group (n = 474). The flow chart of this study is shown in (Figure8).

Table1 summarizes the clinical baseline between the two groups before and after PSM. Although there were significant differences in some patient characteristics between the non-treated group and the treated group before matching, all patient characteristics except alcohol consumption, the level of NT-proBNP, and diuretic using situation were similar between the matched non-treated group and the matched treated group.

Table2 shows the results of comparing HCT, neutrophil count, lymphocyte count, and monocyte count between groups after PSM. Compared to the matched non-treated group, the matched treated group had higher HCT ($P < 0.001$) and lower lymphocyte and monocyte counts ($p = 0.02$, $p < 0.001$). In addition, Supplementary Table1 summarizes the results of HCT, neutrophil count, lymphocyte count, and monocyte count between the two groups before PSM. The SGLT2i treated group had lower HCT ($P < 0.001$) and higher lymphocyte count ($P < 0.001$). There were no inter-group differences between monocyte counts and neutrophil counts ($P = 0.99$, $P = 0.08$).

Due to alcohol consumption between the two groups after PSM, there are still differences in the level of NT-proBNP and diuretic using situations. Therefore, we

used hierarchical analysis to explore the differences in HCT, neutrophil count, lymphocyte count, and monocyte count between the matched treated group and the matched non-treated group in populations with different alcohol consumption, diuretic using situation, and NT-proBNP levels. Categorical variables are directly stratified according to classification. Continuous variables (NT-proBNP) were divided into four groups according to quartile positions. The results showed that the HCT in the matched EM-treated group was higher than that in the matched non-treated group regardless of the stratified situation. In the group who never drank alcohol (Alcohol1), lymphocyte counts in the matched treated group were lower than in the matched non-treated group. In the group with higher NT-proBNP (>2550), the lymphocyte count in the matched treated group was lower than that in the matched non-treated group. In the patients who do not use diuretic treated, the lymphocyte counts of the matched treated group were lower than in the matched non-treated group ($P < 0.001$). In patients treated with diuretics, neutrophil counts were lower in the matched treated group ($P = 0.004$) (Figure8). SGLT2i may play a therapeutic role by regulating HCT and lymphocyte count.

3 Discussion:

Emerging evidence highlights cardiovascular protective effects of SGLT2i, potentially linked to sympathetic inhibition [45], yet their impact on autonomic brain centers remains unexplored. Here, in two salt-related models (DOCA-salt and 8%-HSD models), we showed that EM protected against cardiac remodeling partly by

suppressing central sympathetic outflow. For underlying mechanisms, we found that EM could conduct its protective role via reducing peripheral cytokine-mediated activation of microglia and preventing over-excitation of neuro-endocrine/neurosecretory neurons (Figure9).

Through clinical studies, we have found the effect of EM on lymphocyte count and HCT. This links to what we found in the experimental models. NT-proBNP is an important diagnostic biomarker for of acute heart failure with higher mortality risk. Inflammation appears to be associated with natriuretic peptide (NP) release[46]. It has been reported that BNP level is closely related to extent of LV sympathetic overactivity in heart failure[47, 48]. According to the different affinity of NE to α- and β-adrenergic receptor, increase of sympathetic outflow could induce higher vascular resistance than its effects on heart. Also, elevated cardiac sympathetic tone could further increase cardiac metabolism, reduce cardiac diastole and coronary blood flow, therefore exacerbating the pathological progression. In patients with high NT-proBNP value, EM treatment significantly reduced their number of circulating lymphocytes. EM also significantly reduced lymphocyte count in patients without diuretic treatment, while it markedly lowered neutrophil count in patients received diuretic treatment. In mice, EM also reduced neutrophil count in both DOCA-salt and HSD models (Supplementary Figure3 G, H), similar as their lymphocyte counts. Notably, reduced level of circulating neutrophil might also contribute to less advanced condition of pathological cardiac remodeling. However, for interaction with

the brain cells, it should be lymphocytes (especially the T cells) and associated cytokines, because brain recruitment of neutrophil is very limited in non-infection situation and we did not observe marked change in monocyte level following DOCA-salt or HSD treatment. For T cells, we have shown that DOCA-salt dramatically increase its ratio in peripheral blood mononuclear cells, and ablation of sympatho-excitation, using transgenic mutation that targets the brain, significantly reduced the ratio of both CD3+ and CD8+ T cells[44]. In current study, in both models, we found that EM co-treatment reduced lymphocyte count and the plasma level of IFN-γ, which is produced by lymphocytes. EM has been shown to reduce inflammation in diabetic patients [49-52], but its relationship with lymphocytes and cytotoxic cytokines (*i.e.* IFN-γ) is unknown. IFN-γ is a cytokine that closely correlates to the occurrence and progression of hypertension [16, 53, 54], and it also acts on microglial located in the CNS [55-57], thus promoting neuroinflammation. Reactive microglia in the PVN have been demonstrated to promote excitation of PVN neurons and increase of sympathetic outflow[11, 17-21].

EM co-treatment also increase HCT in the DOCA-salt treated mice (Supplementary Figure3 E, F), similar as in the heart failure patients. Decrease of HCT following DOCA-salt treatment might indicate increase of circulating blood volume, which is similar as the results of some previous studies [58-60]. On the other hand, SGLT2i reduces blood volume. This effect may be caused by the drug's diuretic effect. This has also been confirmed in some clinical studies [61-63]. This suggests

that EM might blunt cardiac remodeling by promoting sodium ion excretion and reducing circulating blood volume. But EM also significantly increased HCT, and lowered neutrophil count, in the patients received diuretics, suggesting additional effect of EM than its diuretic effect. To determine the effect of sodium excretion, we also measured the levels of plasma sodium and osmolality in both DOCA-salt and HSD models. Although the modeling mice had significantly more sodium intake than baseline, their system showed a strong regulatory impact on blood sodium and osmotic pressure (Supplementary Figure3 A-D). The body processes a series of hormones that regulate water-sodium homeostasis, maintaining stable levels of blood sodium and osmotic pressure. Among these hormones, vasopressin is secreted from PVN neurosecretory AVP neurons and plays an essential role in development of DOCA-salt hypertension[24]. Unlike DOCA-salt model, HCT was not altered in mice with HSD treatment, nevertheless, the plasma of level co-peptin, which represents AVP level, was elevated by HSD and brought to the baseline in mice co-treatment of EM, further supporting the involvement of CNS. Accordingly, we think that via facilitating sodium excretion, EM reduced excitation of AVP (Arginine vasopressin) neurons, and less excited AVP neurons secreted lower level of vasopressin, thus further supporting the protective effect of EM.

This study attempted to verify the mechanism by which EM regulates the foot sensation center through clinical samples, but there were several inherent limitations because this study was a single-center retrospective design. First, selection bias may

exist because only patients with complete medical records are included and cases that are more serious or lost to follow-up may be excluded, which may underestimate adverse outcomes. Second, unmeasured confounding factors may affect the results, although we adjusted for available variables. Despite these limitations, the consistency of our findings with previous literature supports its validity.

This study used single-center retrospective study to explore how EM regulates the sympathetic nervous system, acknowledging limitations like selection bias and unmeasured confounders, though consistent findings with prior research support its validity.

4 Conclusion:

In this study, we found that peripheral immune activation contributes to reactive transformation of microglia in the PVN, meanwhile, upregulated ubiquitin-signaling impairs the compensatory activity of ACE2, and this further promoting the hyper-activity of PVN neurons. By targeting peripheral immune activation and over-excitation of neuro-endocrine/neurosecretory neurons, EM reduced sympathetic outflow and plasma vasopressin level, thus introducing protective effect on cardiac pathological remodeling.

5 Methods:

5.1 Antibodies

antibodies	source	indentifier
Tyrosine hydroxylase	Abcam	ab31252
c-Fos	Abcam	c-Fos

IBA1	Abcam	ab208942
CD68	Thermo	MA5-16654
SGLT2	Proteintech	28683-1-AP
NEDD4L	Proteintech	13690-1-AP
GAPDH	CST	2118
Anti rabbit 488	Thermo	A-11008
Anti rat 555	Thermo	A-21434
Anti rabbit HRP	Proteintech	SA00001-2
Anti mouse HRP	Proteintech	SA00001-1

5.2 Stored data

Database	**Number**
GEO dataset	GSE313832
SRA dataset	SUB15305597

5.3 Software and algorithms

Package	**Version**
R	4.2.3
Seurat	4.3.0.1
CellChat	1.6.1

5.4 Experimental Model and Subject Details

This study used male C57BL/6J mice of SPF level at 8 weeks old. They were purchased from Beijing Vital River Laboratory Animal Technology Co., Ltd. (Order No. 44829700009980). The animals were raised in the Experimental Animal Center of Xi'an Jiaotong University under SPF barrier conditions. The animal feed was purchased from Jiangsu Xietong Pharmaceutical Bio-engineering Co., Ltd. (regular feed: SWS9102, 8% NaCl feed: XTNacl-8C). Mice had free access to water and food.

All procedures were approved by the IACUC of Xi'an Jiaotong University (XJTU2021-203), in agreement with the Guide for the Care and Use of Laboratory Animals. Every effort was made to minimize the number of animals used and their suffering. Institutional Animal Care and Use Committees in accordance with the 'Principles of Laboratory Animal Care by the National Society for Medical research and the Guide for the Care and Use of Laboratory Animals' (National Institutes of Health Publication No. 86-23, revised 1996).

5.5 Hypertension Model and High Salt Diet Model

All mice were adaptively fed for 1 week. The DOCA group, DOCA+EM group, DOCA+Hyd group, Sham+EM group and Sham group all underwent right kidney removal. The DOCA group, DOCA+EM group and DOCA+Hyd group underwent Deoxycorticosterone acetate (DOCA) silicone implantation. Anesthesia was induced with isoflurane (3% induction; 1-2% maintenance) using an oxygen flow of 0.5 L/min, and the mice were placed on a heating pad to maintain body temperature at around 37.5□. The mouse was placed in a left lateral position on the operating table, and the skin in the posterior peritoneal area was incised to expose the renal hilum of the right kidney. The blood vessels were ligated with surgical suture at the renal hilum, followed by removal of the right kidney. After surgery, subcutaneous injection of 0.9% saline solution (1mL) was given via backpack skin. One week after recovery, either DOCA, DOCA+EM or DOCA+Hyd groups received subcutaneous implantation of DOCA silicone sheet (containing 1 mg of DOCA per gram body weight). Mice

implanted with DOCA silicone sheets had their drinking water replaced with 1% NaCl solution.

HSD, HSD + EM and normal sodium diet (NSD) groups were fed adaptively for one week. HSD, HSD + EM were fed with a diet containing 8% sodium for 12 weeks. The NSD group was fed with a normal diet (sodium content was 0.45%) for 12 weeks. All mice were given free access to food and water.

All mice treated with EM were administered by daily gavage at a dose of 10mg/kg/day. The dosages of the EM were selected based on the literature. All tissue preparations were performed after euthanasia. Using a precision vaporizer with induction chamber and waste gas scavenger, (indicate the gas anesthetic) will be administered slowly up to [indicate: > 4.5 % (for Isoflurane)] in oxygen and continued until respiratory arrest occurs for > 60 seconds. The chamber is flushed with oxygen only, the animal is removed and rapid removal of (indicate tissues / organs) is performed to assure euthanasia.

5.6 Single-cell RNA-sequencing

5 mice were sacrificed with a lethal dose of isoflurane, and the excess blood was washed off in cold PBS, and the PVN region of each mouse was obtained according to the mouse brain anatomy map. The tissue nucleus was extracted by SHBIO tissue sample nucleus isolation kit (Cat# 52009-10).

Single-cell RNA-Seq libraries were prepared using SeekOne® Digital Droplet (SeekOne® DD) Single Cell 3’ library preparation kit (SeekGene Catalog No.

K00202-0201). The indexed sequencing libraries were cleanup with SPRI beads, quantified by quantitative PCR (KAPA Biosystems KK4824) and then sequenced on Illumina NovaSeq 6000 with PE150 read length or DNBSEQ-T7 platform with PE150 read length.

We used the SeekSoul Tools pipeline to process the cleaned reads and generated the transcript expression matrix. Quality control, clustering, and downstream analysis were performed using Seurat v. 4.3.0.1 in R version 4.2.3 (2023-03-15). Briefly, according to gene, UMI, and mitochondrial gene counts (genes > 100 and < 8000, mitochondria < 5%).

For the clusters, data was normalized and scaled using the NormalizeData function in Seurat with a factor of 10,000. The top 3000 variable genes were selected using the FindVariableFeature function in Seurat, and the data was scaled using the ScaleData function. Cells were clustered using the FindCluster function with 20 principal components and a resolution of 1.0. The cells were then plotted in a two-dimensional space using the 'Unified Manifold Approximation and Projections' (UMAP) technique, and the identities of the cell clusters were determined by their overlap with known marker genes in the literature. 35 clusters were identified as 9 cell types: Mature oligodendrocyte (5,854), Excitatory neuro (11,225), Inhibitory neuro (11,390) , Mix neuro (4,620), Astrocyte (749), Microglial cell (1444), Immature oligodendrocyte (1,264), Endothelial cell & Pericyte (176), Ependymal cell (106). In order to better describe the neuron population, excitatory neurons, inhibitory neurons,

and mixed neurons were further separated and re-clustered. Cells were clustered using the FindCluster function with 20 principal components and a resolution of 0.1.

We performed cell-cell communication analysis using CellChat v1.4.0, which is based on the curated ligand-receptor interaction database (CellChatDB). To perform the analysis, we provided normalized gene expression matrices for PVN tissues as input to CellChat. The computeCommunProb function was used to calculate the total numbers of interactions and interaction strengths, while the computeCommunProbPathway function was used to calculate the communication probabilities for each cell signaling pathway.

5.7 Echocardiography

Transthoracic echocardiography was performed 21 days after DOCA silicone block implantation. Echocardiography was performed under anesthesia with isoflurane (0.25 to 0.50%) supplemented with 100% O2 using a 30MHz probe on Vevo®LAZR-X 3100. Left ventricular mass (LVM) and left ventricular ejection fraction (LVEF) were analyzed from M-mode images.

5.8 Staining of the Heart

After the mice were directly sacrificed, the heart was removed, and the blood washed off the surface in cold PBS. The heart was placed in 4% PFA for 48 hours and then paraffin-embedded sections (10 μm) were performed. The H&E staining kit (Servicebio Cat#: G1076-500ML) and MASSON staining kit (Servicebio Cat#: G1006-20M) were used.

5.9 Immunocytochemistry

After antigen repair with sodium citrate, the paraffin sections of the heart were washed twice with PBS, then 10min was incubated with 0.25%TritonX100 at room temperature, and any non-specific binding was blocked by 10%NGS at room temperature for 1 hour and incubated overnight with TH primary antibody (1:1000, 4 □). After washing with PBS for three times, the rabbits-488 were incubated at room temperature for 1 hour and then washed again with PBS. Finally, anti-staining was performed with DAPI (1-VOL1000-THERMOTIMO-Fisher Science).

For brain tissue, mice were fixed by cardiac perfusion with cold 4%PFA in PBS. After the brain tissue was fixed by 4%PFA and embedded with OCT (SAKURA-4583), the brain map skin of the control mice was sliced (25 μm) and specific parts were taken for immunofluorescence staining. Wash with PBST twice, then incubate 10 min with 0.5%Triton-X100 at room temperature, block any non-specific binding with 10% NGS at room temperature for 1 hour, dilute the primary antibody in proportion and incubate overnight with 4□. After washing with PBS for three times, the corresponding secondary antibody was used to incubate at room temperature for 1 hour, and then cleaned again with PBS. The cell nucleus was stained with DAPI (Thermo Fisher Science Cat#: 62247). The main antibodies used in this study are summarized in in. Finally, the fluorescence microscope (Olympus BX43) was used to capture the image. Using Image J software for image analysis

5.10 Norepinephrine Measurement

Urine samples were collected by bladder massage at the end of the experimental protocol and noradrenaline concentrations were determined using a mouse noradrenaline ELISA kit (Elabscience, Cat#: E-EL-0047) according to the manufacturer's instructions. Noradrenaline levels are normalized by the corresponding creatinine concentration (Elabscience, Cat#: E-BC-K188-M). Normalized noradrenaline concentrations in urine are expressed as ng/ng creatinine.

5.11 Peripheral Blood Cell Counts and Plasma Sodium Detection

After the experimental protocol was completed, the mice were anesthetized with isoflurane and blood was taken through the eyeball. Half of blood was anticoagulation by EDTA anticoagulation. Then the blood was routinely examined by a fully automated three-point population blood cell analyzer (Mindray BC-2800). The remaining blood was anticoagulated by EDTA and centrifuged for 4 □. Follow the manufacturer's instructions to use blood sodium detection kit (Elabscience, Cat#: E-BC-K207-M), MCP-1 test kit (Elabscience, Cat#: E-EL-M3001), co-peptin test kit (JINGMEI BIOTECHNOLOGY, Cat#: JM-12422M1), and IFN-γ test kit (Elabscience, Cat#: E-EL-M0048) to determine the corresponding indicators. The osmotic pressure was detected by an osmometer (Fiske Micro-Osmometer Model 210).

5.12 ACE2 Enzyme Activity Detection

Mice were sacrificed with a lethal dose of isoflurane, and the paraventricular nucleus region of the inferior thalamus was obtained for each mouse according to the

mouse brain anatomy map. ACE2 enzyme activity was determined using the ACE2 enzyme activity detection kit (Beyotime, Cat#: P0319S) according to the manufacturer's instructions.

5.13 Western Blotting

The tissue samples were placed in 8M urea solution (4.8g urea, 10% SDS 5mL 0.5mL 1M Tris PH 7.4 0.5mL, 0.5M EDTA 0.1mL plus H_2O to 10mL) supplemented with a mixture of protease inhibitors (Roche, Cat#: 11697498001) and repeatedly pumped with a 1ml needle. After quantifying the protein concentration by BCA protein assay (Thermo Scientific, Cat#: A55860), the protein sample was mixed with 4 × SDS sample buffers (Thermo Scientific, Cat#: NP0007) and boiled at 65 °C for 10 minutes. 30 μg protein samples were separated on 4-12% MOPS gel (ACE, Cat#: F15412LGel) and transferred to PVDF membrane (Millipore). Seal the imprint in 5% skim milk for 1 hour. On the second day, the protein was detected with specific antibody (diluted by 1purl 1000) and secondary antibody conjugated with HRP (diluted by 1purl 2000). Aim at the rabbit secondary antibody conjugated with Ubr1 (sc-98882) Nedd4-2 and HRP conjugated with GAPDH.

The ECL luminescent solution (MISHUSHENGWU, Cat#: MI00607B) was dripped evenly on the PVDF membrane (Millipore, Cat#: IPVH 00010) and the imaging was carried out by the WB experimental chemiluminescence instrument (Bio-rad, Cat#:0087170). The signal strength was quantified by ImageJ.

5.14 Clinical Study Design

This study is a retrospective single-center clinical study. All participants provided written informed consent before participating in the study. The study was approved by the Institutional Review Board at the Second Affiliated Hospital of Xi'an Jiaotong University (IRB#2024-150). All methods were performed in accordance with the relevant guidelines and regulations.

5.14.1 Study Participants

We reviewed patients diagnosed with heart failure and hospitalized in the Second Affiliated Hospital of Xi'an Jiaotong University from January 2018 to January 2023. The inclusion criteria are: 1) Signed informed consent and was older than 18 years old at the time of signing informed consent; 2) Heart failure was diagnosed within 3 months before enrollment. The exclusion criteria are: 1) Cerebrovascular accident; 2) Fever caused by various reasons, severe infections; 3) Moderate or severe anemia; 4) Uncontrolled hypertension, systolic blood pressure greater than 160mmHg; 5) Renal failure patients; 6) Hyperthyroid endocrine diseases; 7) Take SGLT2i but for less than 1 month.

A total of 1189 patients were included in the study, of which 474 were treated with SGLT2i and 715 were not treated with SGLT2i. We performed PSM (propensity score matching) to match background characteristics between treated and non-treated group. Details of the PSM analysis are described in the Statistical Analysis section. Clinical characteristics and outcomes of the 2 groups were compared before and after

propensity score matching. The primary interests of this study were the HCT, neutrophil count, monocyte count, and lymphocyte count.

Blood pressure, heart rate, weight, and height were all collected on the day of admission. Blood glucose, LDL, serum creatinine, serum uric acid, serum sodium, serum potassium, and NT-proBNP were all measured on the day of admission or after blood was collected on an empty stomach on the morning of the second day. LVEF is the result of cardiac ultrasound during hospitalization. QRS time limit is the result of electrocardiogram measurement on the day of admission.

5.14.2 Statistical Analysis

Data are expressed as a percentage of categorical variables, and continuous variables were subjected to the Wilke-Shapiro test to determine whether the continuous variables were normally distributed. The mean ± standard deviation (SD) of continuously distributed variables is expressed, and non-normally distributed variables are expressed as the median (quartile 1-quartile 3). Normal distributed continuous variables were compared between the 2 groups using a student t-test. Otherwise, continuous variables were compared using the Mann-Whitney U test. Classification variables were compared using Fisher's exact test.

Clinical factors that may be relevant with outcome variables such as sex, age, smoking status, alcohol consumption, diabetes, dyslipidemia, chronic kidney disease, hypertension, angina pectoris, myocardial infarction, atrial fibrillation, renin angiotensin system inhibitors were selected for PSM.ARNI/ACEI/ARB use, diuretics

use, beta-receptor blockers use, aldosterone receptor blockers use, QRS duration, NT-proBNP, serum creatinine value, total cholesterol, LDL, hemoglobin, blood glucose , uric acid on admission were used as independent variables. For matching, the tendency score value of each study subject was calculated, and the caliper value was 0.1. After PSM (1:1), the treated group was matched with the control group, and the balance between the groups was good.

After PSM, HCT, monocyte count, neutrophil count and lymphocyte count in the treated group and control group were tested by Mann-Whitney U test. If there are still differences between the two groups after PSM matching, hierarchical analysis is performed based on this variable and then HCT, monocyte count, neutrophil count and lymphocyte count between groups will be compared.

A P value < 0.05 was considered statistically significant. We analyzed all data by IBM SPSS statistics version 22 (Chicago, IL, USA).

6 Declarations

6.1 Ethics Approval and Consent to Participate

All procedures of anmial research were approved by the IACUC of Xi'an Jiaotong University (XJTU2021-203), in agreement with the Guide for the Care and Use of Laboratory Animals. Every effort was made to minimize the number of animals used and their suffering. Institutional Animal Care and Use Committees in accordance with the 'Principles of Laboratory Animal Care by the National Society

for Medical research and the Guide for the Care and Use of Laboratory Animals' (National Institutes of Health Publication No. 86-23, revised 1996).

The clinical study of this study is a retrospective single-center clinical study. All participants provided written informed consent before participating in the study. The study was approved by the Institutional Review Board at the Second Affiliated Hospital of Xi'an Jiaotong University (IRB#2024-150). All methods were performed in accordance with the relevant guidelines and regulations.

6.2 Consent for publication

We confirm that the manuscript has been read and approved by all authors and that there are no other persons who satisfied the criteria for authorship but are not listed. We further confirm that the order of authors listed in the manuscript has been approved by all of us.

6.3 Data Availability

All requests for raw data, analysed data and materials of this study will be promptly reviewed by the corresponding authors (Dengfeng gao: gaomedic@mail.xjtu.edu.cn) and the Second Affiliated Hospital of Xi'an Jiaotong University.

The raw data of snRNA-seq are available in SRA (SUB15305597). The processed single-cell raw expression matrices that support the findings of this study are available on the Gene Expression Omnibus (GSE313832).

6.4 Competing Interests

All authors declare no competing interests.

6.5 Funding

This work was supported by the National Natural Science Foundation of China (81872563 to Dengfeng Gao and 82100454 to Jiaxi Xu).

6.6 Acknowledgements

We would like to thank Shenglan Yuan for her guidance and assistance in the animal experiment section. Thanks to the medical staff of the Department of Cardiovascular Medicine of the Second Affiliated Hospital of Xi`an Jiaotong University for their help in the clinical research part. Thanks to all the patients who participated in the clinical research.

Reference：

[1] Gibb AA, Hill BG. Metabolic coordination of physiological and pathological cardiac remodeling. Circulation Research, 2018, 123: 107-128

[2] Patel SM, Kang YM, Im K*, et al.* Sodium-glucose cotransporter-2 inhibitors and major adverse cardiovascular outcomes: A smart-c collaborative meta-analysis. Circulation, 2024, 149: 1789-1801

[3] Udell JA, Yuan Z, Rush T*, et al.* Cardiovascular outcomes and risks after initiation of a sodium glucose cotransporter 2 inhibitor results from the easel population-based cohort study (evidence for cardiovascular outcomes with sodium glucose cotransporter 2 inhibitors in the real world). Circulation, 2018, 137: 1450-1459

696 [4] Kumar K, Kheiri B, Simpson TF, *et al.* Sodium-glucose cotransporter-2 inhibitors in heart
697 failure: A meta-analysis of randomized clinical trials. American Journal of Medicine, 2020, 133:
698 E625-E630
699 [5] Dyck JRB, Sossalla S, Hamdani N, *et al.* Cardiac mechanisms of the beneficial effects of
700 sglt2 inhibitors in heart failure: Evidence for potential off-target effects. Journal of Molecular
701 and Cellular Cardiology, 2022, 167: 17-31
702 [6] Cowie MR, Fisher M. Sglt2 inhibitors: Mechanisms of cardiovascular benefit beyond
703 glycaemic control. Nature Reviews Cardiology, 2020, 17: 761-772
704 [7] Zhang DY, Anderson AS. The sympathetic nervous system and heart failure. Cardiol Clin,
705 2014, 32: 33-45, vii
706 [8] Allen WE, Blosser TR, Sullivan ZA, *et al.* Molecular and spatial signatures of mouse
707 brain aging at single-cell resolution. Cell, 2023, 186: 194-208 e118
708 [9] Cao K, Qiu L, Lu X, *et al.* Microglia modulate general anesthesia through p2y(12)
709 receptor. Current biology : CB, 2023, 33: 2187-2200 e2186
710 [10] Li P, Ma S, Ma X, *et al.* Reversal of neurovascular decoupling and cognitive impairment
711 in patients with end-stage renal disease during a hemodialysis session: Evidence from a
712 comprehensive fmri analysis. Human brain mapping, 2023, 44: 989-1001
713 [11] Wang YL, Zhu H, Pan YT, *et al.* Dendritic cell mineralocorticoid receptor controls blood
714 pressure by regulating t helper 17 differentiation: Role of the plcbeta1/4-stat5-nf-kappab
715 pathway. Eur Heart J, 2025, 46: 1335-1351

716 [12] Zhu Q, Xiao L, Cheng G, *et al.* Self-maintaining macrophages within the kidney
717 contribute to salt and water balance by modulating kidney sympathetic nerve activity. Kidney
718 Int, 2023, 104: 324-333
719 [13] Perrotta M, Lori A, Carnevale L, *et al.* Deoxycorticosterone acetate-salt hypertension
720 activates placental growth factor in the spleen to couple sympathetic drive and immune
721 system activation. Cardiovasc Res, 2018, 114: 456-467
722 [14] Lu X, Crowley SD. Actions of immune cells in the hypertensive kidney. Curr Opin
723 Nephrol Hypertens, 2020, 29: 515-522
724 [15] Ye SJ, Huang H, Han X, *et al.* Dectin-1 acts as a non-classical receptor of ang ii to
725 induce cardiac remodeling. Circulation Research, 2023, 132: 707-722
726 [16] Benson LN, Liu Y, Wang X, *et al.* The ifnγ-pdl1 pathway enhances cd8t-dct interaction to
727 promote hypertension. Circulation Research, 2022, 130: 1550-1564
728 [17] Dong Z, Hou L, Luo W, *et al.* Myocardial infarction drives trained immunity of monocytes,
729 accelerating atherosclerosis. Eur Heart J, 2024, 45: 669-684
730 [18] McMoneagle E, Zhou J, Zhang S, *et al.* Neuronal k(+)-cl(-) cotransporter kcc2 as a
731 promising drug target for epilepsy treatment. Acta pharmacologica Sinica, 2024, 45: 1-22
732 [19] Santisteban MM, Schaeffer S, Anfray A, *et al.* Meningeal interleukin-17-producing t cells
733 mediate cognitive impairment in a mouse model of salt-sensitive hypertension. Nat Neurosci,
734 2024, 27: 63-77

735 [20] Wei B, Cheng G, Bi Q*, et al.* Microglia in the hypothalamic paraventricular nucleus sense
736 hemodynamic disturbance and promote sympathetic excitation in hypertension. Immunity,
737 2024,
738 [21] Yu Y, Weiss RM, Wei SG. Interleukin 17a contributes to blood-brain barrier disruption of
739 hypothalamic paraventricular nucleus in rats with myocardial infarction. Journal of the
740 American Heart Association, 2024, 13: e032533
741 [22] Nielsen SF, Duus CL, Buus NH*, et al.* Randomized, placebo-controlled trial on the renal
742 and systemic hemodynamic effects of empagliflozin. Kidney international reports, 2025, 10:
743 134-144
744 [23] Umanath K, Testani JM, Lewis JB. "Dip" in egfr: Stay the course with sglt-2 inhibition.
745 Circulation, 2022, 146: 463-465
746 [24] Basting T, Lazartigues E. Doca-salt hypertension: An update. Curr Hypertens Rep, 2017,
747 19: 32
748 [25] Tyler M Basting JX, Srinivas Sriramula, Snigdha Murkerjee, and Eric Lazartigues. Knock-
749 down of adam17 in glutamatergic or pre-autonomic neurons attenuates development of
750 neurogenic hypertension. The FASEB Journal, 2017, 31:
751 [26] Grobe JL, Buehrer BA, Hilzendeger AM*, et al.* Angiotensinergic signaling in the brain
752 mediates metabolic effects of deoxycorticosterone (doca)-salt in c57 mice. Hypertension,
753 2011, 57: 600-607

754 [27] Grobe JL, Buehrer BA, Hilzendeger AM, *et al.* Angiotensinergic signaling in the brain
755 mediates metabolic effects of deoxycorticosterone (doca)-salt in c57 mice. Hypertension,
756 2011, 57: 600-607
757 [28] Albo D, Akay CL, Marshall CL, *et al.* Neurogenesis in colorectal cancer is a marker of
758 aggressive tumor behavior and poor outcomes. Cancer, 2011, 117: 4834-4845
759 [29] Hao X, Chen J, Luo Z, *et al.* Trpv1 activation prevents high-salt diet-induced nocturnal
760 hypertension in mice. Pflügers Archiv - European Journal of Physiology, 2011, 461: 345-353
761 [30] Li KX, Lu YM, Xu ZH, *et al.* Neuregulin 1 regulates excitability of fast-spiking neurons
762 through kv1.1 and acts in epilepsy. Nat Neurosci, 2011, 15: 267-273
763 [31] Bal-Price A, Brown GC. Inflammatory neurodegeneration mediated by nitric oxide from
764 activated glia-inhibiting neuronal respiration, causing glutamate release and excitotoxicity.
765 The Journal of neuroscience : the official journal of the Society for Neuroscience, 2001, 21:
766 6480-6491
767 [32] Chen X, Firulyova M, Manis M, *et al.* Microglia-mediated t cell infiltration drives
768 neurodegeneration in tauopathy. Nature, 2023, 615: 668-677
769 [33] Chen X, Gao R, Song Y, *et al.* Astrocytic at1r deficiency ameliorates abeta-induced
770 cognitive deficits and synaptotoxicity through beta-arrestin2 signaling. Progress in
771 neurobiology, 2023, 228: 102489
772 [34] Lyu Y, Huo J, Jiang W, *et al.* Empagliflozin ameliorates cardiac dysfunction in heart
773 failure mice via regulating mitochondrial dynamics. European Journal of Pharmacology, 2023,
774 942: 175531

775 [35] Pongratz G, Straub RH. [role of the sympathetic nervous system in chronic inflammation].
776 Z Rheumatol, 2023, 82: 451-461
777 [36] Robert SM, Reeves BC, Kiziltug E, *et al.* The choroid plexus links innate immunity to csf
778 dysregulation in hydrocephalus. Cell, 2023, 186: 764-785 e721
779 [37] Seo DO, O'Donnell D, Jain N, *et al.* Apoe isoform- and microbiota-dependent
780 progression of neurodegeneration in a mouse model of tauopathy. Science, 2023, 379:
781 eadd1236
782 [38] Weng Y, Chen N, Zhang R, *et al.* An integral blood-brain barrier in adulthood relies on
783 microglia-derived pdgfb. Brain, behavior, and immunity, 2024, 115: 705-717
784 [39] Xu Z, Hu SW, Zhou Y, *et al.* Corticotropin-releasing factor neurones in the
785 paraventricular nucleus of the hypothalamus modulate isoflurane anaesthesia and its
786 responses to acute stress in mice. British journal of anaesthesia, 2023,
787 [40] Xue L, Cui SM, Yang FH, *et al.* Myocardial senescence induced by inactivation aldh2-
788 sirt1-gata4 pathway involves in heart remolding after acute infarction. Circulation, 2016, 134:
789 [41] Mazher M, Blessing O, Mona E, *et al.* Nedd4-2 up-regulation is associated with ace2
790 ubiquitination in hypertension. Cardiovasc Res, 2023, 119:
791 [42] Mohammed M, Ogunlade B, Elgazzaz M, *et al.* Nedd4-2 upregulation is associated with
792 ace2 ubiquitination in hypertension. Cardiovasc Res, 2023, 119: 2130-2141
793 [43] Mukerjee S, Gao H, Xu J, *et al.* Ace2 and adam17 interaction regulates the activity of
794 presympathetic neurons. Hypertension, 2019, 74: 1181-1191

795 [44] Xu J, Molinas AJR, Mukerjee S, *et al.* Activation of adam17 (a disintegrin and
796 metalloprotease 17) on glutamatergic neurons selectively promotes sympathoexcitation.
797 Hypertension, 2019, 73: 1266-1274
798 [45] Spallone V, Valensi P. Sglt2 inhibitors and the autonomic nervous system in diabetes: A
799 promising challenge to better understand multiple target improvement. Diabetes &
800 Metabolism, 2021, 47: 101224
801 [46] Fish-Trotter H, Ferguson JF, Patel N, *et al.* Inflammation and circulating natriuretic
802 peptide levels. Circ Heart Fail, 2020, 13: e006570
803 [47] Sakata K, Iida K, Mochiduki N, *et al.* Brain natriuretic peptide (bnp) level is closely
804 related to the extent of left ventricular sympathetic overactivity in chronic ischemic heart
805 failure. Intern Med, 2009, 48: 393-400
806 [48] Tsukuda K, Mogi M, Iwanami J, *et al.* Cognitive deficit in amyloid-beta-injected mice was
807 improved by pretreatment with a low dose of telmisartan partly because of peroxisome
808 proliferator-activated receptor-gamma activation. Hypertension, 2009, 54: 782-787
809 [49] Maayah ZH, Ferdaoussi M, Takahara S, *et al.* Empagliflozin suppresses inflammation
810 and protects against acute septic renal injury. Inflammopharmacology, 2021, 29: 269-279
811 [50] Gohari S, Reshadmanesh T, Khodabandehloo H, *et al.* The effect of empagliflozin on
812 markers of inflammation in patients with concomitant type 2 diabetes mellitus and coronary
813 artery disease: The empa-card randomized controlled trial. Diabetol Metab Syndr, 2022, 14:
814 170

815 [51] Benedetti R, Chianese U, Papulino C, *et al.* Unlocking the power of empagliflozin:
816 Rescuing inflammation in hyperglycaemia- exposed human cardiomyocytes through
817 comprehensive multi-level analysis. Eur J Heart Fail, 2025,
818 [52] Fu J, Xu H, Wu F, *et al.* Empagliflozin inhibits macrophage inflammation through ampk
819 signaling pathway and plays an anti-atherosclerosis role. Int J Cardiol, 2022, 367: 56-62
820 [53] Benson LN, Liu Y, Deck K, *et al.* Ifn-γ contributes to the immune mechanisms of
821 hypertension. Kidney360, 2022, 3: 2164-2173
822 [54] Shokoples BG, Comeau K, Higaki A, *et al.* Angiotensin ii-induced a steeper blood
823 pressure elevation in il-23 receptor-deficient mice: Role of interferon-γ-producing t cells.
824 Hypertension Research, 2023, 46: 40-49
825 [55] Ding X, Yan Y, Li X, *et al.* Silencing ifn-γ binding/signaling in astrocytes versus microglia
826 leads to opposite effects on central nervous system autoimmunity. J Immunol, 2015, 194:
827 4251-4264
828 [56] He Z, Yang Y, Xing Z, *et al.* Intraperitoneal injection of ifn-γ restores microglial
829 autophagy, promotes amyloid-β clearance and improves cognition in app/ps1 mice. Cell
830 Death & Disease, 2020, 11: 440
831 [57] Zhang H, Zhang T, Wang D, *et al.* Ifn-γ regulates the transformation of microglia into
832 dendritic-like cells via the erk/c-myc signaling pathway during cerebral ischemia/reperfusion in
833 mice. Neurochemistry International, 2020, 141: 104860
834 [58] Griffin M, Rao VS, Ivey-Miranda J, *et al.* Empagliflozin in heart failure. Circulation, 2020,
835 142: 1028-1039

836 [59] Shikuma J, Sakakura K, Sugiyama-Takahashi M*, et al.* Hematocrit elevation after sglt2
837 inhibitor administration may be associated with the degree of proximal tubular damage.
838 Medicine (Baltimore), 2022, 101: e31122
839 [60] Tian Q, Guo K, Deng J*, et al.* Effects of sglt2 inhibitors on haematocrit and haemoglobin
840 levels and the associated cardiorenal benefits in t2dm patients: A meta-analysis. J Cell Mol
841 Med, 2022, 26: 540-547
842 [61] Wilcox CS. Antihypertensive and renal mechanisms of sglt2 (sodium-glucose linked
843 transporter 2) inhibitors. Hypertension, 2020, 75: 894-901
844 [62] Omar M, Jensen J, Burkhoff D*, et al.* Effect of empagliflozin on blood volume
845 redistribution in patients with chronic heart failure and reduced ejection fraction: An analysis
846 from the empire hf randomized clinical trial. Circulation: Heart Failure, 2022, 15: e009156
847 [63] Sen T, Scholtes R, Greasley PJ*, et al.* Effects of dapagliflozin on volume status and
848 systemic haemodynamics in patients with chronic kidney disease without diabetes: Results
849 from dapasalt and diamond. Diabetes Obes Metab, 2022, 24: 1578-1587
850

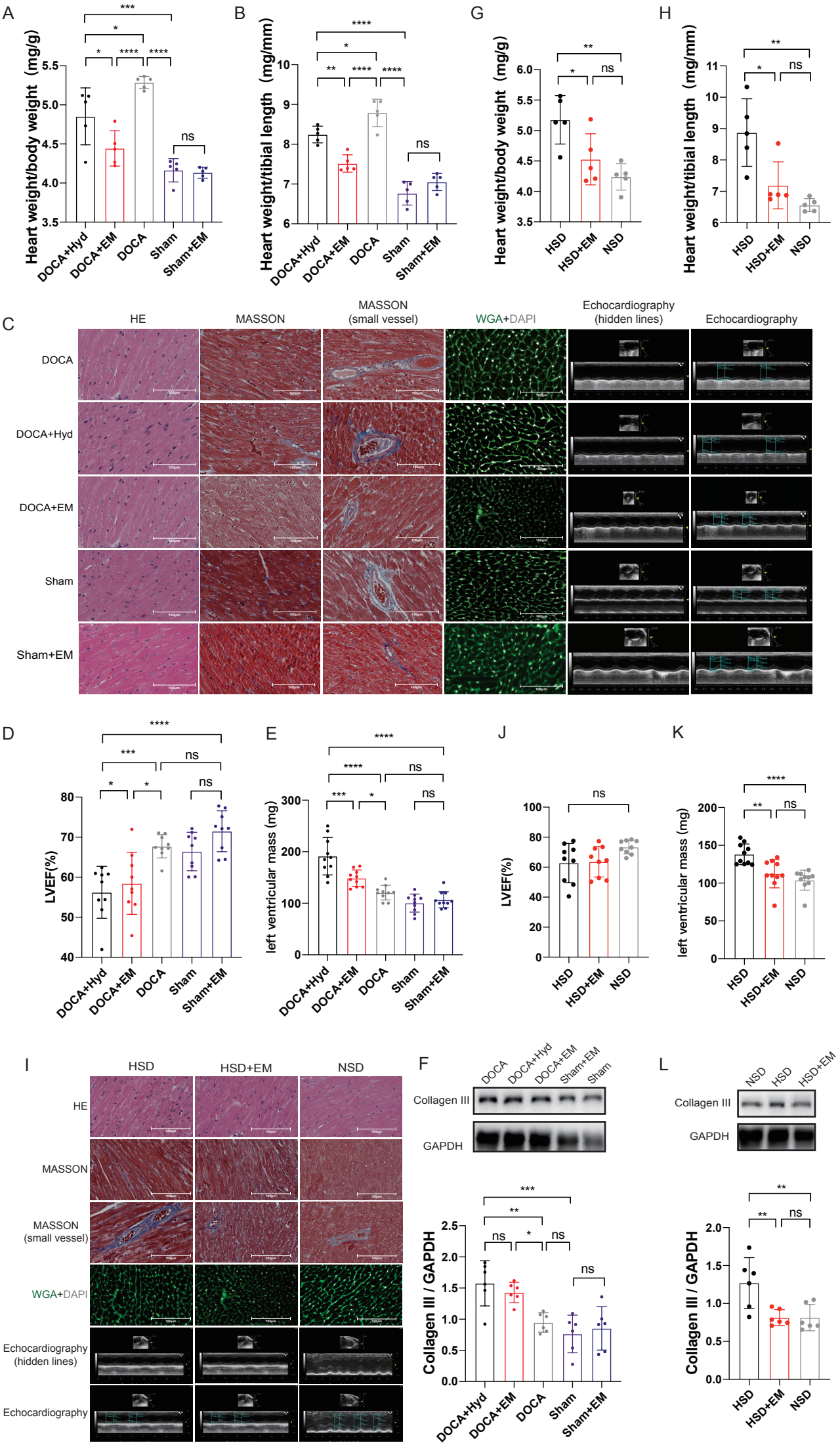
A
Heart weight/body weight (mg/g)
DOCA+Hyd
DOCA+EM
DOCA
Sham
Sham+EM
ns
B
Heart weight/tibial length (mg/mm)
G
Heart weight/body weight (mg/g)
HSD
HSD+EM
NSD
H
Heart weight/tibial length (mg/mm)
C
HE
MASSON
MASSON (small vessel)
WGA+DAPI
Echocardiography (hidden lines)
Echocardiography
D
LVEF(%)
E
left ventricular mass (mg)
J
LVEF(%)
K
left ventricular mass (mg)
I
F
Collagen III
GAPDH
Collagen III / GAPDH
L

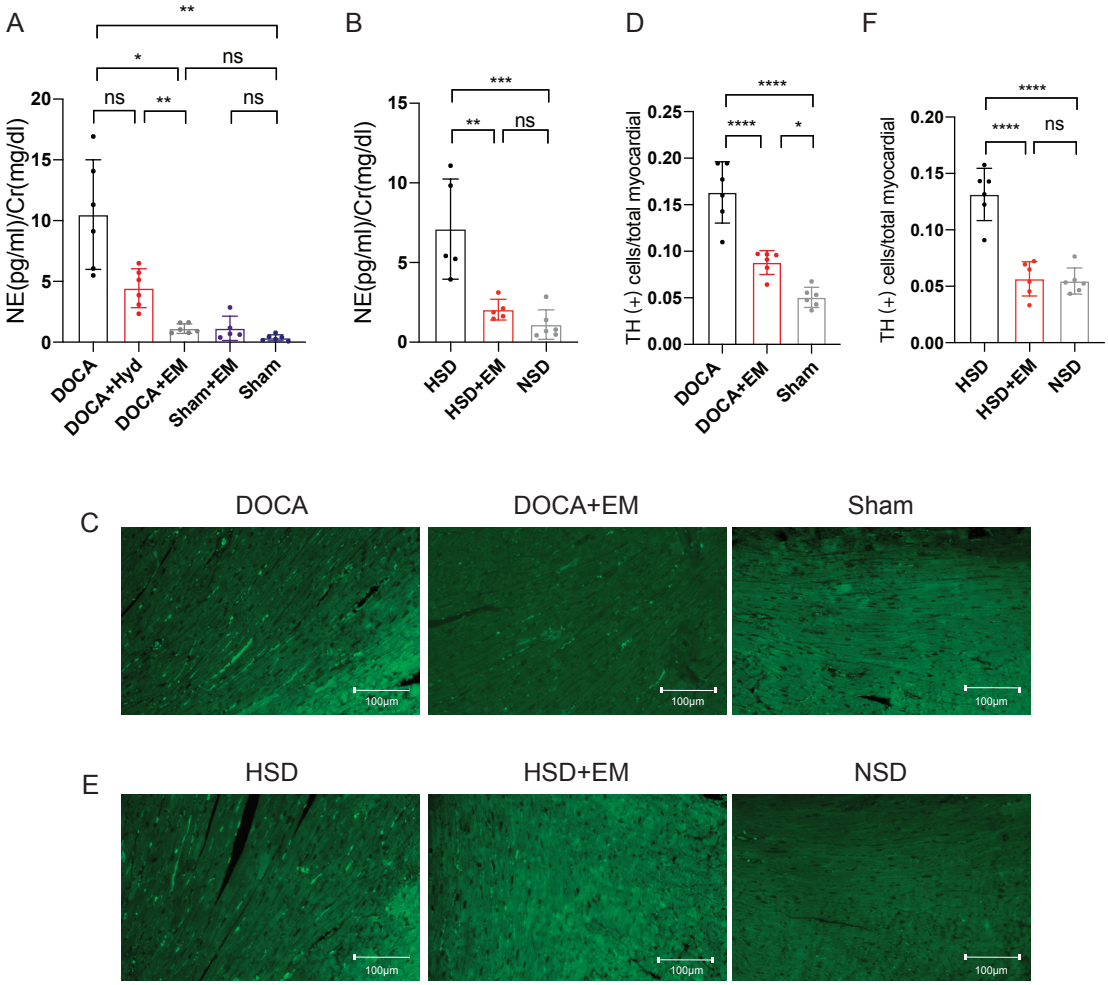
A
NE(pg/ml)/Cr(mg/dl)
DOCA
DOCA+Hyd
DOCA+EM
Sham+EM
Sham
B
NE(pg/ml)/Cr(mg/dl)
HSD
HSD+EM
NSD
D
TH (+) cells/total myocardial
DOCA
DOCA+EM
Sham
F
TH (+) cells/total myocardial
HSD
HSD+EM
NSD
C
DOCA
DOCA+EM
Sham
E
HSD
HSD+EM
NSD
100μm

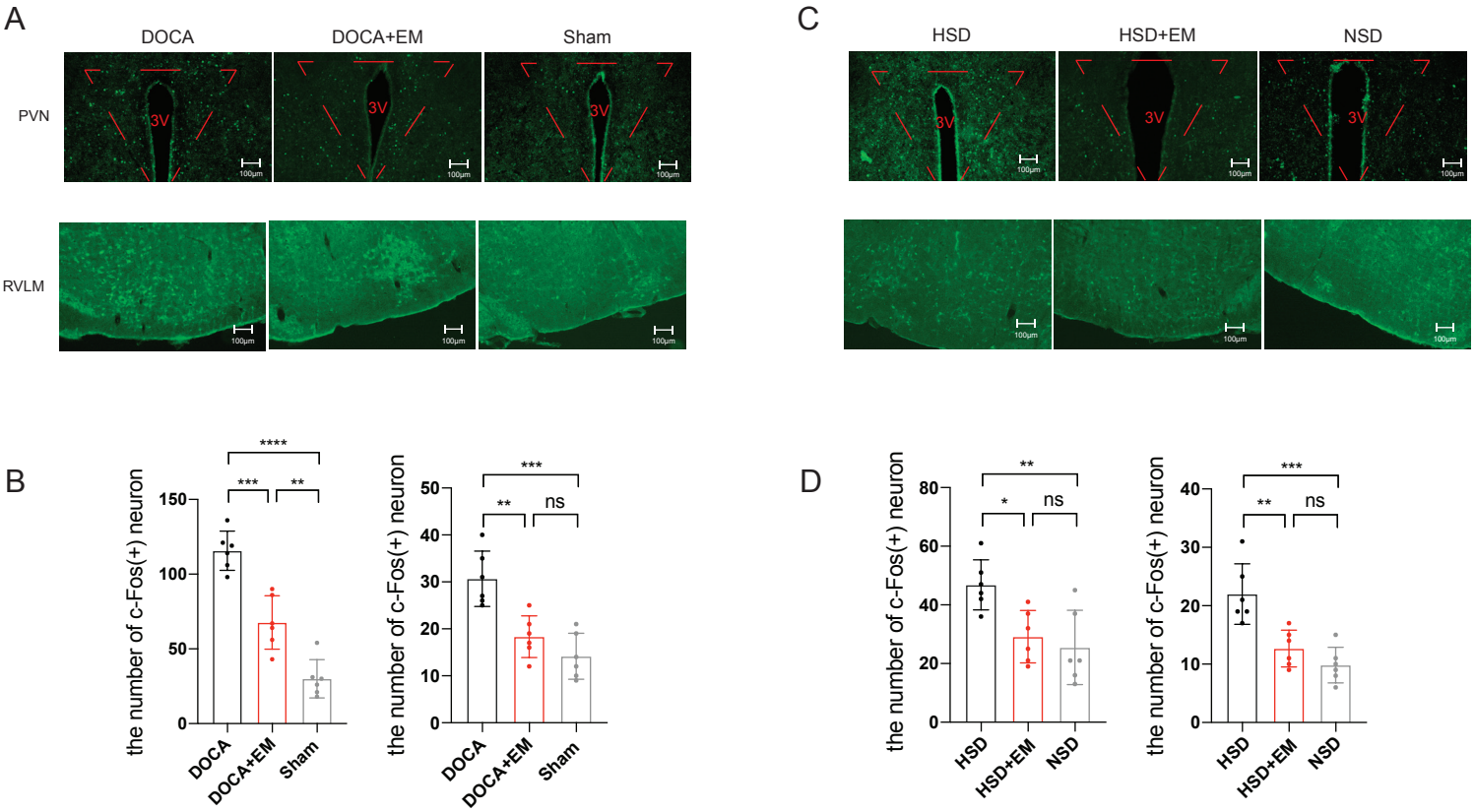
A
DOCA
DOCA+EM
Sham
PVN
RVLM
3V
100μm
C
HSD
HSD+EM
NSD
B
the number of c-Fos(+) neuron
****
***
**
ns
DOCA
DOCA+EM
Sham
D
*
HSD
HSD+EM
NSD

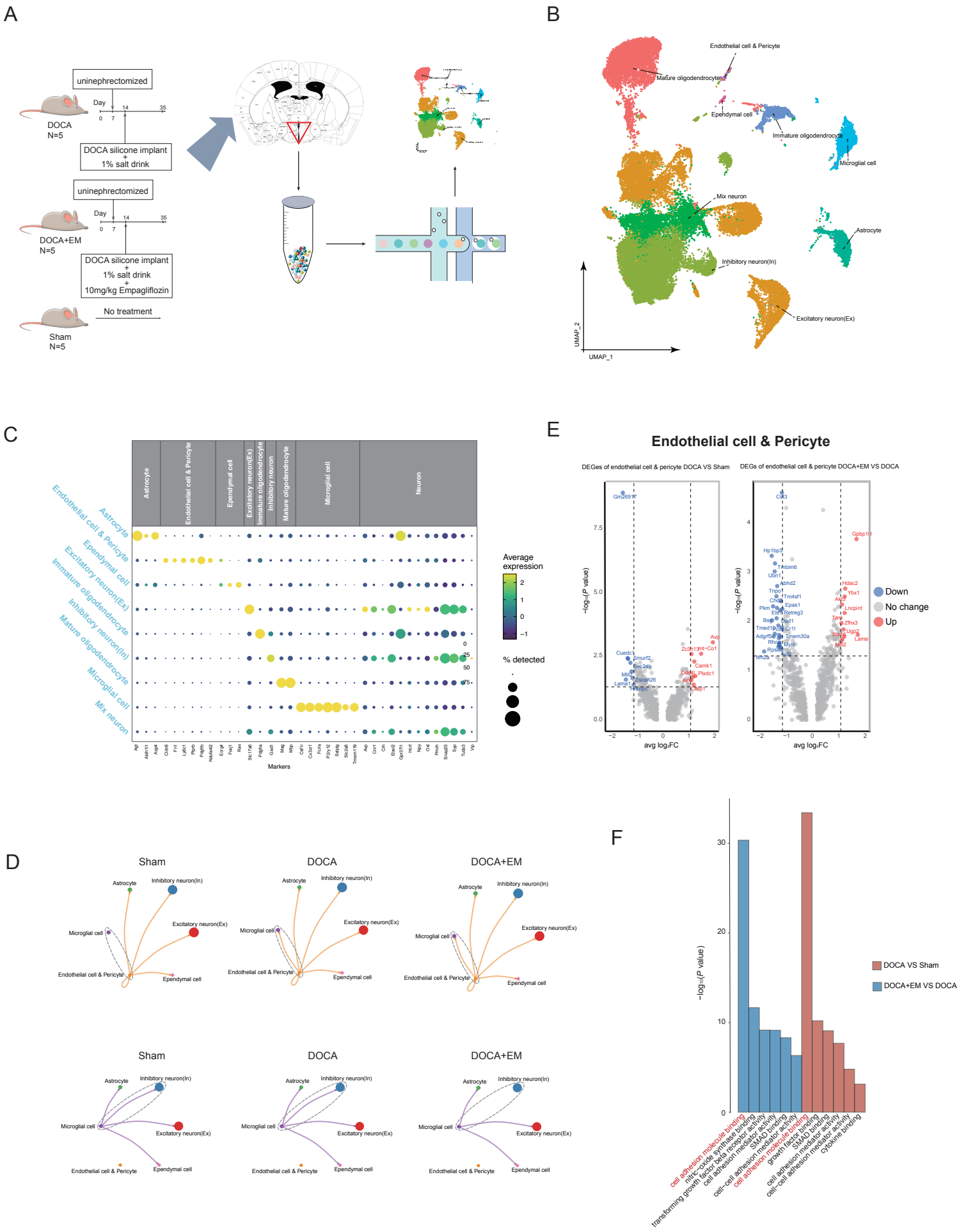
A
uninephrectomized
DOCA
N=5
Day
0 7 14 35
DOCA silicone implant
+
1% salt drink
uninephrectomized
DOCA+EM
N=5
Day
0 7 14 35
DOCA silicone implant
+
1% salt drink
+
10mg/kg Empagliflozin
No treatment
Sham
N=5
B
Endothelial cell & Pericyte
Mature oligodendrocyte
Ependymal cell
Immature oligodendrocyte
Microglial cell
Mix neuron
Astrocyte
Inhibitory neuron(In)
Excitatory neuron(Ex)
UMAP_2
UMAP_1
C
Astrocyte
Endothelial cell & Pericyte
Ependymal cell
Immature oligodendrocyte
Mature oligodendrocyte
Microglial cell
Neuron
Endothelial cell & Pericyte
Astrocyte
Ependymal cell
Excitatory neuron(Ex)
Immature oligodendrocyte
Inhibitory neuron(In)
Mature oligodendrocyte
Microglial cell
Mix neuron
Markers
Average expression
% detected
E
Endothelial cell & Pericyte
DEGes of endothelial cell & pericyte DOCA VS Sham
DEGs of endothelial cell & pericyte DOCA+EM VS DOCA
−log10(P value)
avg log2FC
Down
No change
Up
D
Sham
DOCA
DOCA+EM
Astrocyte
Inhibitory neuron(In)
Excitatory neuron(Ex)
Microglial cell
Endothelial cell & Pericyte
Ependymal cell
F
−log10(P value)
DOCA VS Sham
DOCA+EM VS DOCA
cell adhesion molecule binding
nitric-oxide synthase binding
transforming growth factor beta receptor binding
cell adhesion mediator activity
SMAD binding
cell−cell adhesion mediator activity
cell adhesion molecule binding
growth factor binding
SMAD binding
cell adhesion mediator activity
cell−cell adhesion mediator activity
cytokine binding

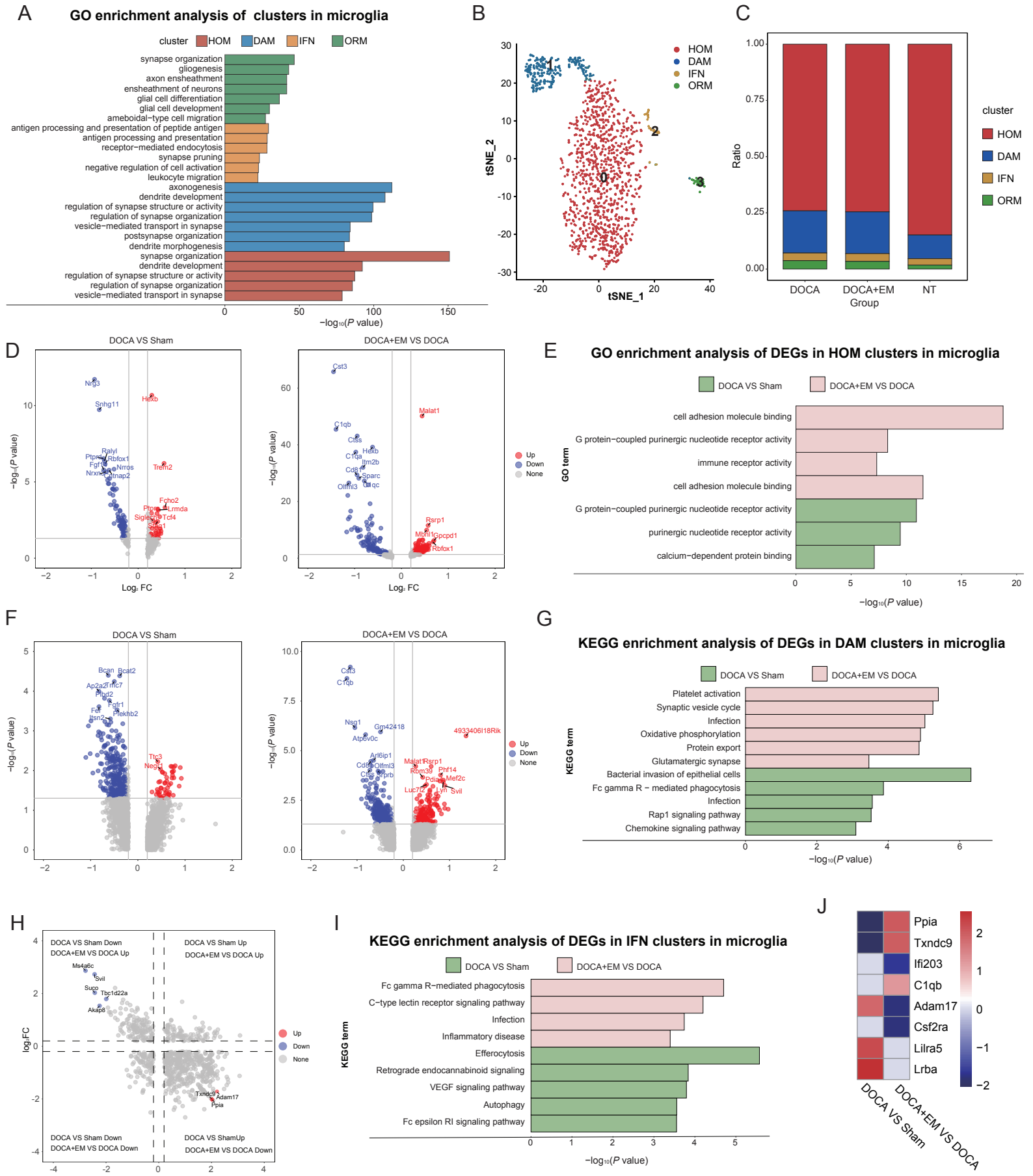
A
GO enrichment analysis of clusters in microglia
cluster HOM DAM IFN ORM
synapse organization
gliogenesis
axon ensheathment
ensheathment of neurons
glial cell differentiation
glial cell development
ameboidal−type cell migration
antigen processing and presentation of peptide antigen
antigen processing and presentation
receptor−mediated endocytosis
synapse pruning
negative regulation of cell activation
leukocyte migration
axonogenesis
dendrite development
regulation of synapse structure or activity
regulation of synapse organization
vesicle−mediated transport in synapse
postsynapse organization
dendrite morphogenesis
synapse organization
dendrite development
regulation of synapse structure or activity
regulation of synapse organization
vesicle−mediated transport in synapse
−log10(P value)
B
HOM
DAM
IFN
ORM
tSNE_2
tSNE_1
C
Ratio
cluster
HOM
DAM
IFN
ORM
DOCA
DOCA+EM
NT
Group
D
DOCA VS Sham
DOCA+EM VS DOCA
−log10(P value)
Log2 FC
Up
Down
None
E
GO enrichment analysis of DEGs in HOM clusters in microglia
DOCA VS Sham
DOCA+EM VS DOCA
GO term
cell adhesion molecule binding
G protein−coupled purinergic nucleotide receptor activity
immune receptor activity
cell adhesion molecule binding
G protein−coupled purinergic nucleotide receptor activity
purinergic nucleotide receptor activity
calcium−dependent protein binding
−log10(P value)
F
DOCA VS Sham
DOCA+EM VS DOCA
−log10(P value)
Up
Down
None
G
KEGG enrichment analysis of DEGs in DAM clusters in microglia
DOCA VS Sham
DOCA+EM VS DOCA
KEGG term
Platelet activation
Synaptic vesicle cycle
Infection
Oxidative phosphorylation
Protein export
Glutamatergic synapse
Bacterial invasion of epithelial cells
Fc gamma R − mediated phagocytosis
Infection
Rap1 signaling pathway
Chemokine signaling pathway
−log10(P value)
H
DOCA VS Sham Down
DOCA+EM VS DOCA Up
DOCA VS Sham Up
DOCA+EM VS DOCA Up
DOCA VS Sham Down
DOCA+EM VS DOCA Down
DOCA VS ShamUp
DOCA+EM VS DOCA Down
logFC
Up
Down
None
I
KEGG enrichment analysis of DEGs in IFN clusters in microglia
DOCA VS Sham
DOCA+EM VS DOCA
KEGG term
Fc gamma R−mediated phagocytosis
C−type lectin receptor signaling pathway
Infection
Inflammatory disease
Efferocytosis
Retrograde endocannabinoid signaling
VEGF signaling pathway
Autophagy
Fc epsilon RI signaling pathway
−log10(P value)
J
Ppia
Txndc9
Ifi203
C1qb
Adam17
Csf2ra
Lilra5
Lrba
DOCA VS Sham
DOCA+EM VS DOCA

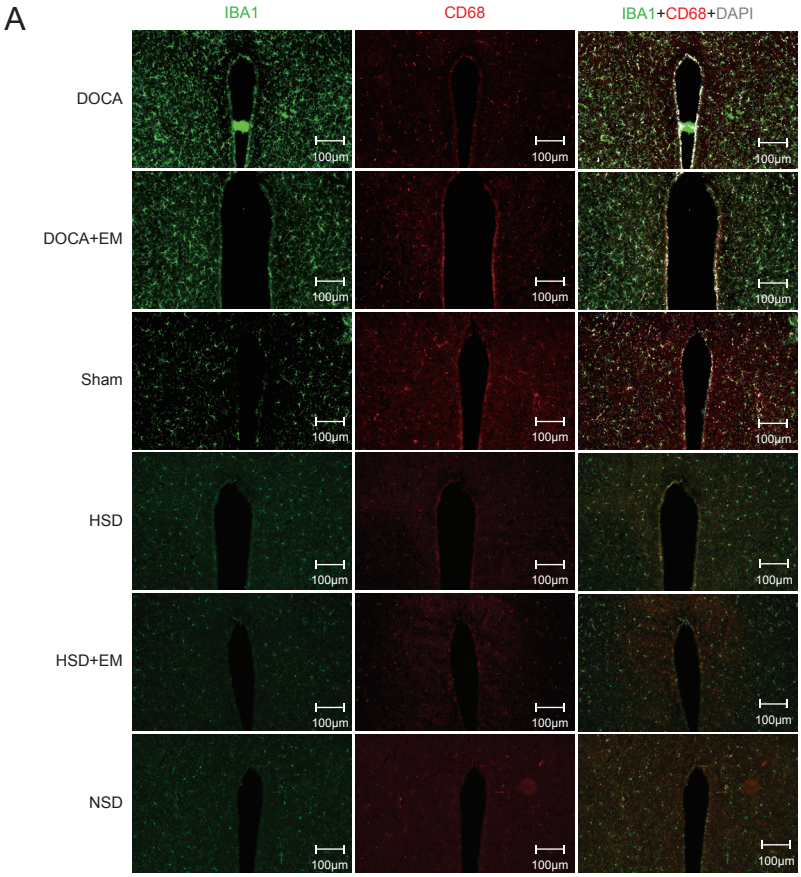
A
IBA1
CD68
IBA1+CD68+DAPI
DOCA
DOCA+EM
Sham
HSD
HSD+EM
NSD
100μm

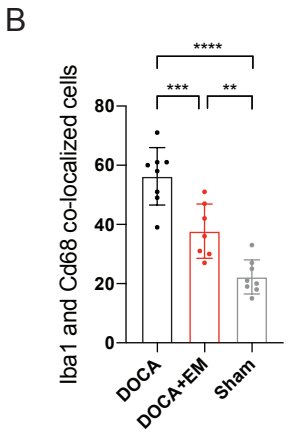
B
Iba1 and Cd68 co-localized cells
****
***
**
DOCA
DOCA+EM
Sham

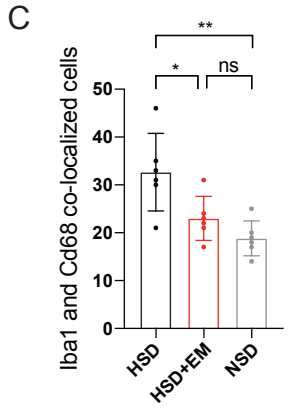
C
Iba1 and Cd68 co-localized cells
**
*
ns
HSD
HSD+EM
NSD

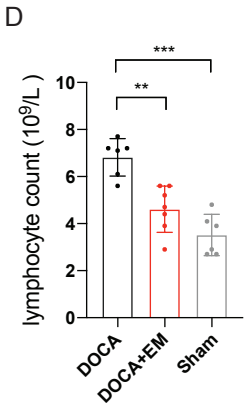
D
lymphocyte count (10⁹/L)
***
**
DOCA
DOCA+EM
Sham

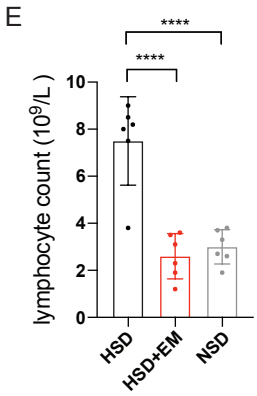
E
lymphocyte count (10⁹/L)
****
****
HSD
HSD+EM
NSD

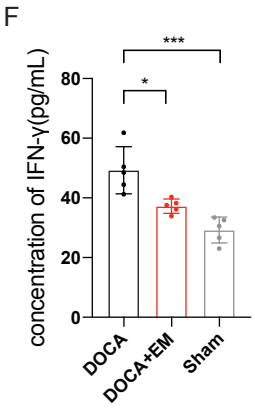
F
concentration of IFN-γ(pg/mL)
***
*
DOCA
DOCA+EM
Sham

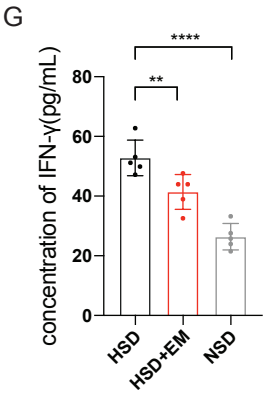
G
concentration of IFN-γ(pg/mL)
****
**
HSD
HSD+EM
NSD

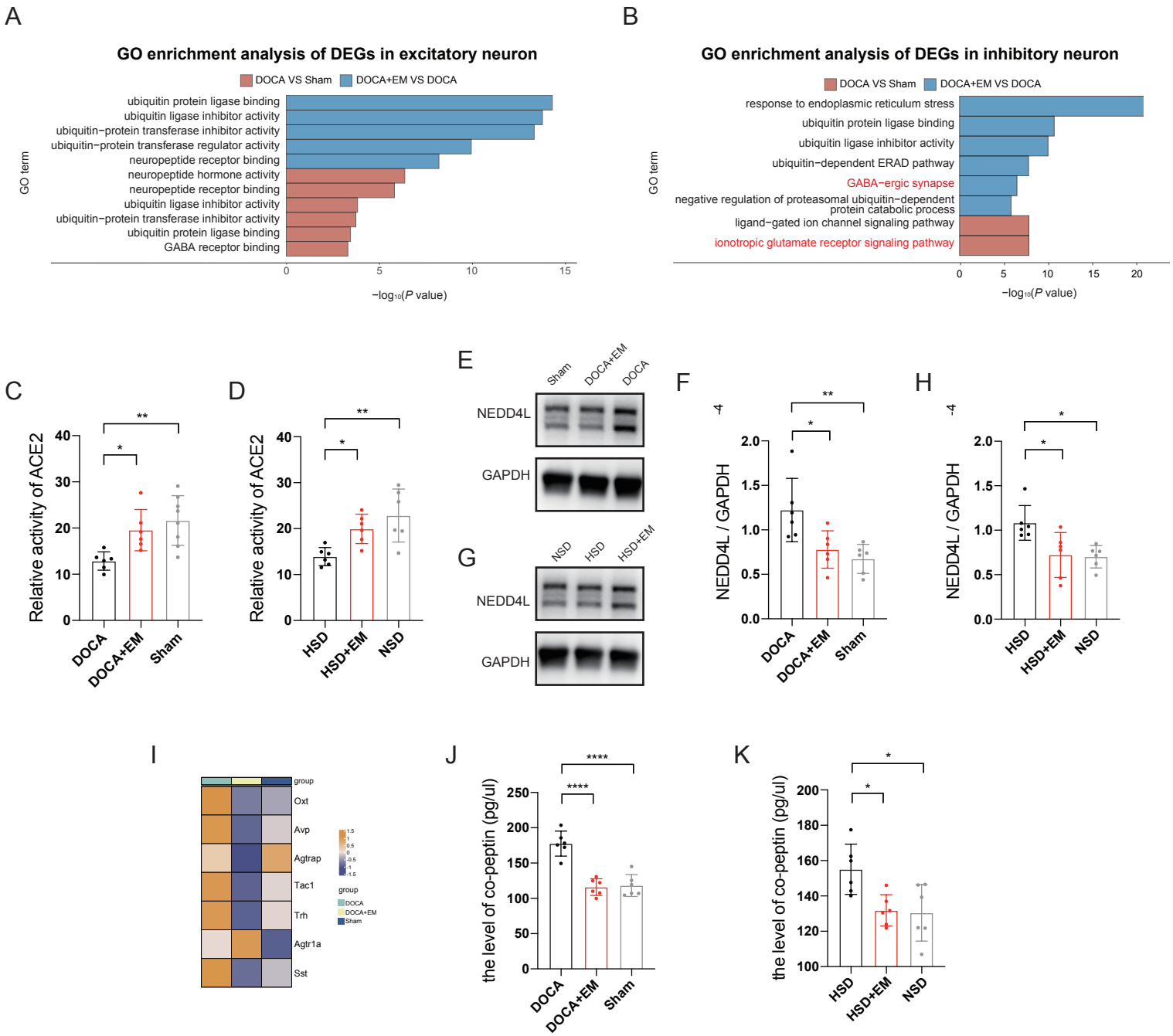
A
GO enrichment analysis of DEGs in excitatory neuron
DOCA VS Sham
DOCA+EM VS DOCA
GO term
ubiquitin protein ligase binding
ubiquitin ligase inhibitor activity
ubiquitin−protein transferase inhibitor activity
ubiquitin−protein transferase regulator activity
neuropeptide receptor binding
neuropeptide hormone activity
neuropeptide receptor binding
ubiquitin ligase inhibitor activity
ubiquitin−protein transferase inhibitor activity
ubiquitin protein ligase binding
GABA receptor binding
−log10(P value)
B
GO enrichment analysis of DEGs in inhibitory neuron
DOCA VS Sham
DOCA+EM VS DOCA
GO term
response to endoplasmic reticulum stress
ubiquitin protein ligase binding
ubiquitin ligase inhibitor activity
ubiquitin−dependent ERAD pathway
GABA−ergic synapse
negative regulation of proteasomal ubiquitin−dependent protein catabolic process
ligand−gated ion channel signaling pathway
ionotropic glutamate receptor signaling pathway
−log10(P value)
C
Relative activity of ACE2
DOCA
DOCA+EM
Sham
D
Relative activity of ACE2
HSD
HSD+EM
NSD
E
Sham
DOCA+EM
DOCA
NEDD4L
GAPDH
G
NSD
HSD
HSD+EM
NEDD4L
GAPDH
F
NEDD4L / GAPDH
DOCA
DOCA+EM
Sham
H
NEDD4L / GAPDH
HSD
HSD+EM
NSD
I
group
Oxt
Avp
Agtrap
Tac1
Trh
Agtr1a
Sst
group
DOCA
DOCA+EM
Sham
J
the level of co-peptin (pg/ul)
DOCA
DOCA+EM
Sham
K
the level of co-peptin (pg/ul)
HSD
HSD+EM
NSD

A

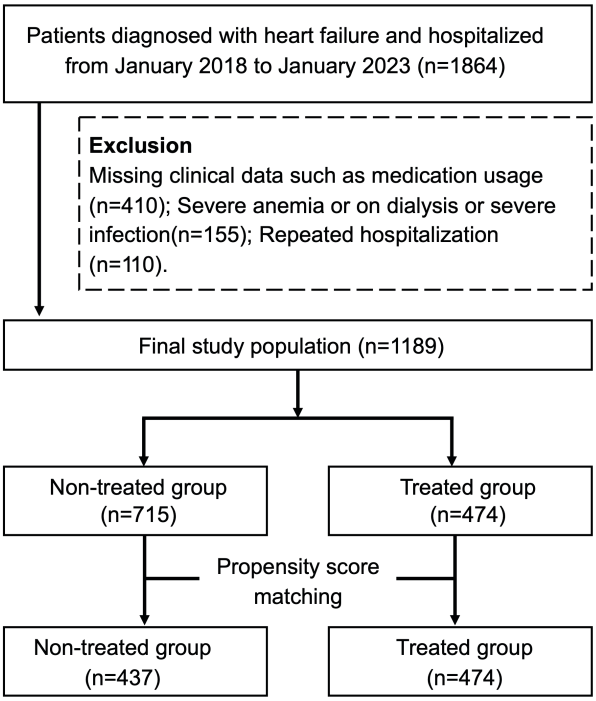
Patients diagnosed with heart failure and hospitalized from January 2018 to January 2023 (n=1864)
Exclusion
Missing clinical data such as medication usage (n=410); Severe anemia or on dialysis or severe infection(n=155); Repeated hospitalization (n=110).
Final study population (n=1189)
Non-treated group (n=715)
Treated group (n=474)
Propensity score matching
Non-treated group (n=437)
Treated group (n=474)

B

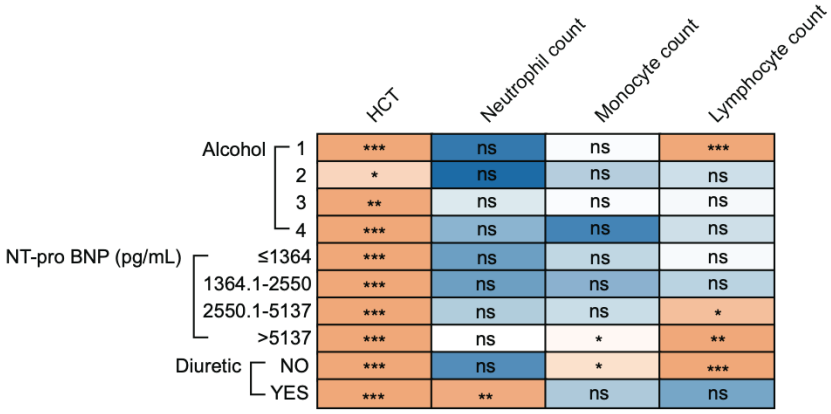
HCT
Neutrophil count
Monocyte count
Lymphocyte count
Alcohol
1
2
3
4
NT-pro BNP (pg/mL)
≤1364
1364.1-2550
2550.1-5137
>5137
Diuretic
NO
YES

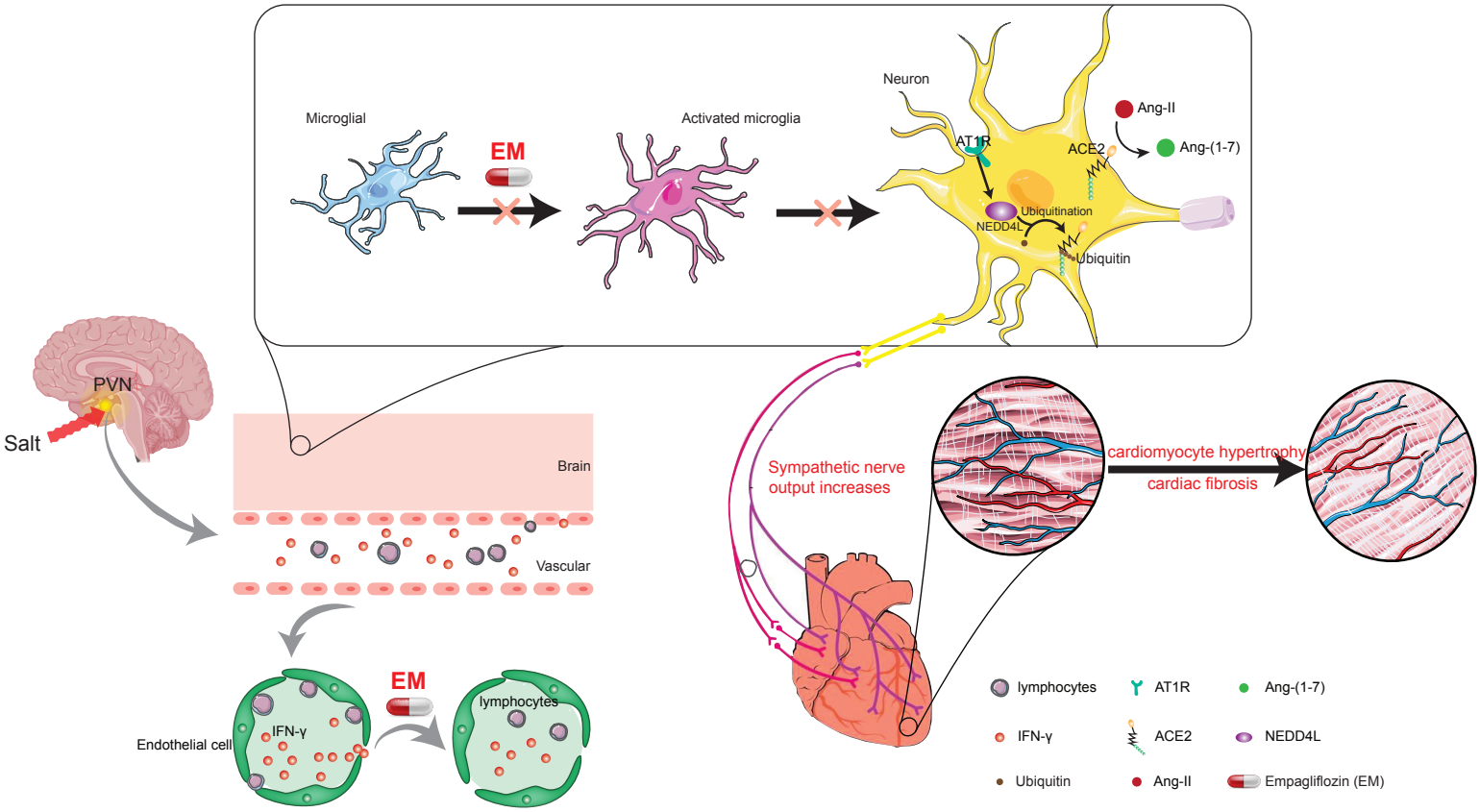
Microglial
EM
Activated microglia
Neuron
AT1R
ACE2
Ang-II
Ang-(1-7)
Ubiquitination
NEDD4L
Ubiquitin
PVN
Salt
Brain
Vascular
Endothelial cell
IFN-γ
EM
lymphocytes
Sympathetic nerve
output increases
cardiomyocyte hypertrophy
cardiac fibrosis
lymphocytes
AT1R
Ang-(1-7)
IFN-γ
ACE2
NEDD4L
Ubiquitin
Ang-II
Empagliflozin (EM)

Table 1 Baseline comparison of the treated group and non-treated group before and after propensity score matching

		Non-treat group	treat group	p value	Matcher non-treat group	Matched treat group	p value
		n=715 (60.1%)	n=474 (39.9%)		n=437 (48%)	n=474 (52%)	
patient characteristics							
Sex (n)	M	479	341	0.71	299	341	0.246
	F	236	133		138	133	
Age(years)		68(59-75)	66(58-66)	0.032	67(57-74)	58(66-73)	0.701
Weight(kg)		65(60-75)	70(60-79.25)	0.04	67(60-77)	70(60-79.25)	0.286
Height(cm)		168(160-172)	170(162-174.25)	0.03	169(160-173)	170(162-174.25)	0.182
Hypertension	No	279	206	0.127	186	206	0.785
	Yes	436	268		251	268	
2 type diabetes	No	493	252	<0.001	270	252	0.009
	Yes	222	222		167	222	
Dyslipidemia	No	638	421	0.771	383	421	0.582
	Yes	76	53		54	53	
angina	No	551	390	0.03	363	390	0.754
	Yes	164	84		74	84	
MI	No	527	343	0.609	320	343	0.77
	Yes	188	131		117	131	
AF	No	464	315	0.579	285	315	0.694
	Yes	251	159		152	159	
Chronic kidney disease	No	141	386	0.621	363	386	0.52
	Yes	574	88		74	88	
Smoke[a]	1	460	298	0.859	286	298	0.677
	2	85	58		52	58	
	3	12	11		6	11	
	4	158	107		93	107	
Drink[b]	1	605	378	0.004	363	378	0.006
	2	11	13		2	13	
	3	16	28		13	28	
	4	83	55		59	55	
SBP (mmHg)		129(113-145)	129(110.75-142.25)	0.516	127(112-142.5)	78(69-88)	0.788
DBP (mmHg)		76(69-87)	78(69-88)	0.426	76(69-87)	78(69-88)	0.343
Heart rate (bmp)		80(70-94)	82(71-97)	0.088	80(70-95)	97(96-98)	0.277
SpO_2 (%)		97(96-98)	97(96-98)	0.479	97(96-98)	97(96-98)	0.418
QRS duration (ms)		96(86-108)	100(90-118)	<0.001	98(88-114)	100(90-118)	0.083
Blood glucose (mmol/L)		5.45(4.8-6.181)	6.181(4.99-6.838)	<0.001	5.81(5.005-6.49)	6.18(4.99-6.84)	0.137
Hemoglobin		135(120-147)	135.5(122-150)	0.229	136(122-148)	135.5(122-150)	0.767
NT-proBNP (pg/mL)		2095(1193-4153)	2896.5(1570.5-5595)	<0.001	2216(1248.5-4851)	2896.5(1570.5-5595)	0.002
Serum Na^+ (mmol/L)		140.1(138-142.3)	140.4(138-142.3)	0.385	140(137.8-142)	140.4(138-142.3)	0.07
Serum K^+ (mmol/L)		4.1(3.8-4.5)	4.1(3.8-4.4)	0.505	4.1(3.8-4.5)	4.1(3.8-4.4)	0.365

Serum Cr (mmol/L)		83.8(68.6-104.7)	83.65(70.25-100.925)	0.533	82.9(68-102)	83.65(70.25-100.93)	0.685
Total cholesterol (mmol/L)		3.5(2.86-4.2)	3.445(2.848-4.215)	0.638	3.55(2.85-4.285)	3.45(2.85-4.22)	0.392
LDL		2.01(1.46-2.58)	1.995(1.5-2.635)	0.552	2.1(1.5-2.65)	2.0(1.5-2.64)	0.55
Serum uric acid (mmol/L)		389.701(311-429)	389.701(329.75-434)	0.245	389.701(324-437.5)	389.70(329.75-434)	0.948
LVEF (%)		54(42-62)	47(37-58)	<0.001	49.95(38-60)	47(37-58)	0.057
ACEI/ARB/ARIN	No	19	3	0.011	6	3	0.259
	Yes	696	471		431	471	
MRA	No	217	69	<0.001	69	69	0.604
	Yes	498	405		368	405	
Beta blocker	No	31	11	0.065	12	11	0.683
	Yes	684	463		425	463	
Diuretic	No	434	352	<0.001	253	352	<0.001
	Yes	281	122		184	122	

[a] 1: Never or smoking occasionally;

2: Quit smoking more than half a year;

3: Quit smoking less than half a year;

4: Smoking every day.

[b] 1: Never;

2: Drinking occasionally (less than 3 times a week);

3: Regular alcohol consumption (about 3 times a week);

4: Quit drinking.

MI: myocardial infarction

AF: atrial fibrillation

SBP: systolic blood pressure.

DBP: diastolic blood pressure.

LDL: low density lipoprotein.

LVEF: left ventricular ejection fraction.

MRA: mineralcorticoid recept antagonis.

ACEI/ARB/ARIN: angiotensin-converting enzyme inhibitors/ Angiotensin II receptor antagonist/ angiotensin receptor-neprilysin inhibitor.

Table 2 Comparison of HCT and peripheral immune cell counts between the treated group and non-treated group after propensity matching score

		Matched non-treat group	Matched treat group	*P* value
	n=911	n=437 (48%)	n=474 (52%)	
HCT		39.9(37-43.4)	43(39.63-46.1)	<0.001
Neutrophil count		4.29(3.34-5.58)	4.18(3.19-5.31)	0.22
Monocyte count		0.52(0.4-0.68)	0.49(0.39-0.63)	0.02
Lymphocyte count		1.52(1.19-1.91	1.39(1-1.77)	<0.001